JOURNAL OF PETROLOGY | VOLUME 46 | NUMBER 2 | PAGES 197–230 | 2005 | doi:10.1093/petrology/egh062

093394
33

Petrogenesis of Pre-caldera Mafic Lavas, Jemez Mountains Volcanic Field (New Mexico, USA)

J. A. WOLFF[1]*, M. C. ROWE[2], R. TEASDALE[3], J. N. GARDNER[4], F. C. RAMOS[5] AND C. E. HEIKOOP[6]†

[1]DEPARTMENT OF GEOLOGY, WASHINGTON STATE UNIVERSITY, PULLMAN, WA 99164, USA
[2]DEPARTMENT OF GEOSCIENCES, OREGON STATE UNIVERSITY, 104 WILKINSON HALL, CORVALLIS, OR 97331, USA
[3]DEPARTMENT OF GEOLOGICAL AND ENVIRONMENTAL SCIENCES, CALIFORNIA STATE UNIVERSITY, CHICO, CA 95929, USA
[4]EARTH AND ENVIRONMENTAL SCIENCES, LOS ALAMOS NATIONAL LABORATORY, LOS ALAMOS, NM 87545, USA
[5]DEPARTMENT OF EARTH SCIENCES, UNIVERSITY OF CALIFORNIA, SANTA CRUZ, CA 95064, USA
[6]DEPARTMENT OF GEOLOGY, MCMASTER UNIVERSITY, 1280 MAIN STREET WEST, HAMILTON, ONTARIO L8S 4M1, CANADA

RECEIVED MARCH 30, 2004; ACCEPTED SEPTEMBER 20, 2004
ADVANCE ACCESS PUBLICATION DECEMBER 10, 2004

The Miocene–Quaternary Jemez Mountains volcanic field (JMVF), the site of the Valles caldera, lies at the intersection of the Jemez lineament, a Proterozoic suture, and the Cenozoic Rio Grande rift. Parental magmas are of two types: K-depleted silica-undersaturated, derived from the partial melting of lithospheric mantle with residual amphibole, and tholeiitic, derived from either asthenosphere or lithospheric mantle. Variability in silica-undersaturated basalts reflects contributions of melts derived from lherzolite and pyroxenite mantle, representing heterogeneous lithosphere associated with the suture. The K depletion is inherited by fractionated, crustally contaminated derivatives (trachytes and magnesites), leading to distinctive incompatible trace element signatures, with Th/(Nb, Ta) and La/(Nb, Ta) greater than, but K/(Nb, Ta) similar to, Bulk Silicate Earth. These compositions dominate the mafic and intermediate lavas, and the JMVF is therefore derived largely, and perhaps entirely, from melting of fertile continental Jemez lineament lithosphere during rift-related extension. Significant variations in Pb and Nd isotopic ratios ($^{206}Pb/^{204}Pb$ = 17·20–18·93; $^{143}Nd/^{144}Nd$ = 0·51244–0·51272) result from crustal contamination, whereas $^{87}Sr/^{86}Sr$ is low and relatively uniform (0·7040–0·7043). We compare the effects of contamination by low $^{87}Sr/^{86}Sr$ crust with assimilation of high $^{87}Sr/^{86}Sr$ granitoid by partial melting, with Sr retained in a feldspathic residue. Both models satisfactorily reproduce the isotopic features of the rocks, but the lack of a measurable Eu anomaly in most JMVF mafic lavas is difficult to reconcile with a major role for residual plagioclase during petrogenesis.

KEY WORDS: *Jemez Mountains volcanic field; Rio Grande rift; lithospheric mantle; crustal contamination; trace elements; radiogenic isotopes*

INTRODUCTION

The Jemez Mountains volcanic field (JMVF) in New Mexico is well known as the site of the Valles caldera, one of three large Quaternary continental rhyolitic caldera systems in the USA: the other two are Long Valley and Yellowstone. The JMVF has a history of volcanism reaching back over 20 Myr prior to the caldera-forming eruptions of the Bandelier Tuff, involving magma compositions ranging from nephelinite to high-silica rhyolite. This longevity of active volcanism, despite significant westward movement of the North American continent during this time, indicates that the controls on the location of JMVF volcanism reside within the lithosphere. Our purpose is to examine the bulk-rock geochemistry of pre-Valles JMVF mafic volcanic rocks with the

*Corresponding author. Telephone: +1 509 335 2825. Fax: +1 509 335 3316. Email: jawolff@mail.wsu.edu
†Present address: 510 Garvey Lane, White Rock, NM 87544, USA

© Oxford University Press 2005; all rights reserved

14363
AUG 14 2006

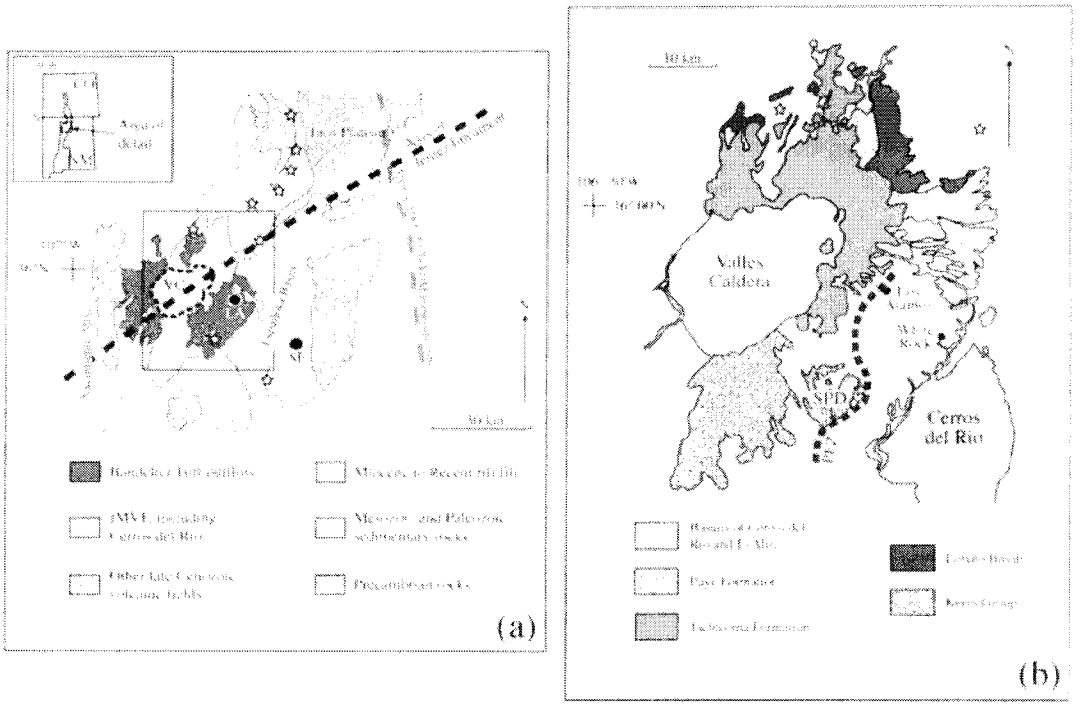

Fig. 1. Regional and Jemez Mountains volcanic field (JMVF) geological maps, showing features referred to in the text. (a) The JMVF and adjacent Rio Grande rift in northern New Mexico. The Colorado Plateau lies west and NW of the Rio Grande rift and the Jemez lineament, respectively. Outcrops of mafic lavas in the Santa Fe Group (including those discussed by Gibson *et al.* (1993)) are indicated by stars. Box outlines area of (b). VC, Valles caldera; SF, Santa Fe; LA, Los Alamos. Inset: NM, New Mexico; CO, Colorado. (b) Outcrop of pre-Tesuque Group rocks discussed in the text, simplified after Smith *et al.* (1970), Manley (1982) and Goff *et al.* (1990). Blank areas represent either cover by Tesuque Group or formations lying beneath the base of the JMVF, including the Santa Fe Group. Outcrop patterns in the Keres Group are intricate, and not represented at the formation level. The El Alto lavas are the 'Basalt of Cerros del Rio and El Alto' that lie near the northern extremity of the map. Stars as in (a). PEZ, trace of the main portion of the Pajarito fault zone that forms the western boundary of the Española basin. SPD, St. Peter's Dome.

intention of identifying mantle components that have played important roles in magmatism, the extent to which the mantle-derived magmas have been compositionally modified by interaction with regional crust, and to describe their contribution to the construction of a moderate-sized (~2000 km^3), long-lived volcanic field that ultimately hosted caldera-forming eruptions of catastrophic magnitude. We focus on lavas with < 57% SiO_2; silicic rocks will be discussed in a future paper. Although lavas in this compositional range make up less than 10% of the exposed JMVF pile, they span most of the lifetime of the field, and a mafic component is often present in the much more voluminous mixed andesites and dacites; there can be little doubt that the JMVF is 'fundamentally basaltic' (Hildreth, 1981). This paper is intended to provide a basis for future, more detailed studies of the temporal development of the JMVF, and to provide a foundation for understanding the petrogenesis of the climactic rhyolitic magmas.

The earliest lavas in the area, dated at 25–16·5 Ma, are interbedded with Santa Fe Group basin-fill sediments of the adjacent Rio Grande rift (Bailey *et al.*, 1969; Smith *et al.*, 1970; Gardner *et al.*, 1986; Woldegabriel *et al.*, 2003). Subsequent activity between 13 and 6 Ma built a large (1000 km^3) andesite-dominated volcanic ridge on the basin margin (Fig. 1), now represented by lavas of the Paliza Canyon Formation and other units of the Keres Group (Bailey *et al.*, 1969; Smith *et al.*, 1970), mostly exposed in the southern Jemez Mountains. The northern part of the Jemez Mountains consists mainly of lavas making up the Polvadera Group of Bailey *et al.* (1969). The earliest, basalt-dominated, Polvadera activity occurred between 14 and 7 Ma (Goff *et al.*, 1989; Aldrich & Dethier, 1990), to produce the Lobato Basalt. Coincident with a lull in crustal extension (Gardner *et al.*, 1986), the dacite-dominated Tschicoma Formation was erupted between 7 and 2 Ma (Goff *et al.*, 1989) in the northern and northeastern Jemez. The latter stages of Polvadera Group activity shifted towards rhyolitic compositions between 4 and 2 Ma (Turbeville *et al.*, 1989). During the same period, mafic volcanism around the eastern and northern margins of the JMVF (Smith *et al.*,

1970; Baldridge, 1979) produced the Cerros del Rio and El Alto volcanic fields, which consist of lavas and scoria with 15–64% SiO_2. It should be emphasized that JMVF formations exhibit considerable stratigraphic, geochronological and geographical overlap. Prior work has indicated that the pre-caldera volcanic rocks record varying styles and degrees of interaction between mantle-derived magmas and continental crust (Gardner, 1985; Singer & Kudo, 1986; Duecker *et al.*, 1991; Ellison *et al.*, 1996; Wolff *et al.*, 2000).

The Tewa Group of Bailey *et al.* (1969) consists of the rhyolitic products of the Valles caldera, which are dominated by the Bandelier Tuff (Fig. 1a). The major caldera-forming units of the Bandelier Tuff, the Otowi and Tshirege Members, erupted at 1·61 and 1·23 Ma, respectively (Izett & Obradovich, 1994; Spell *et al.*, 1996). Smaller volume rhyolitic lavas and tuffs were emplaced before, between, and after the Bandelier eruptions. Aspects of the petrology and geochemistry of the caldera-related rhyolites have been considered by Smith (1979), Stix *et al.* (1988), Spell & Kyle (1989), Spell *et al.* (1990, 1993, 1996), Dunbar & Hervig (1992), Stix & Gorton (1995), Wolff & Gardner (1995), Stimac (1996), Wolff *et al.* (1999, 2002) and Wolff & Ramos (2003).

REGIONAL TECTONIC SETTING, GEOLOGY, AND MAGMATISM

The Rio Grande rift is the only major manifestation of Basin-and-Range extension that lies east of the Colorado Plateau. It consists of a north–south-trending series of Cenozoic *en echelon* sedimentary basins that bisects New Mexico and southern Colorado. The rift cuts across regional trends in mid-Proterozoic metamorphic and granitic rocks and overlying Upper Paleozoic to Cenozoic sedimentary rocks. The JMVF is built on the western shoulder of the Española basin, at the intersection of the rift and the Jemez lineament (Fig. 1a). The latter is an alignment of late Cenozoic volcanic fields extending from SE Arizona to NE New Mexico, which coincides with the surface boundary of a suture zone complex between the Proterozoic Southern Yavapai (1·8–1·7 Ga) and Mazatzal (1·65 Ga) lithospheric provinces (Shaw & Karlstrom, 1999; Karlstrom *et al.*, 2002). Compared with the abundant volcanism along the lineament, the Rio Grande rift is relatively starved of magma; indeed, the JMVF is by far the largest volcanic field associated with the rift.

Recent geophysical investigations, summarized by Duecker *et al.* (2001) and Karlstrom *et al.* (2002), have shed light on lithospheric structure beneath the Jemez lineament just east of the rift (CD-ROM project seismic line, Fig. 1a). Seismic reflection data show south-dipping mid-crustal reflections that project toward a south-dipping mantle boundary broadly coincident with the Jemez lineament. The boundary separates high-velocity mantle to the south from low-velocity mantle to the north, extends to >200 km depth, and is interpreted as the Southern Yavapai–Mazatzal suture (Karlstrom *et al.*, 2002). The low-velocity mantle to the north of the lineament is one of a number of NE-trending similarly aligned features beneath the lineament, which Duecker *et al.* (2001) argued are more significant regional mantle structures than those resulting from rifting. Significantly for magma genesis, the low-velocity feature is internally layered, suggesting that it resides in the lithosphere. It extends from the Moho (at 40–50 km) to a depth of 120 km, the inferred base of the lithosphere.

Rifting in northern New Mexico began around 30 Ma with crustal extension, locally exceeding 100% (Morgan *et al.*, 1986), over a width of ~170 km. The original Española basin, coincident with but broader than the present basin, formed with a western boundary fault in the Nacimiento Mountains (Aldrich, 1986; Morgan *et al.*, 1986). Following a period of quiescence from at least 18 to 13 Ma, extension was reinitiated within a narrower zone (~50 km) along the pre-existing axis, with the western rift boundary trending north–south through the center of the JMVF. A further lull in extensional activity between 7 and 4 Ma (Gardner *et al.*, 1986) ended with the development of the Pajarito fault zone (Fig. 1), marking another eastward shift of the Española basin's western boundary. Temperatures may exceed 900°C in the lower crust beneath the rift (Baldridge *et al.*, 1984; Clarkson & Reiter, 1984; Morgan & Golombek, 1984). This is within the range of solidus temperatures of crustal lithologies, hence thermal perturbations caused by intrusions of mantle-derived primitive basaltic magma into the sub-rift crust are very likely to induce partial melting of the Proterozoic crustal rocks.

The JMVF is built on a substrate of Upper Paleozoic sedimentary strata that rest on the Proterozoic basement, which consists of granitoid and metamorphic rocks locally dated at 1·62–1·44 Ga (Brookins & Laughlin, 1983). The Paleozoic succession is associated with basin development during the ancestral Rocky Mountains orogeny (Pazzaglia *et al.*, 1999) and is overlain by a veneer of Cenozoic sedimentary units, the uppermost of which is the eastward-thickening rift-filling Santa Fe Group (Bailey *et al.*, 1969; Smith *et al.*, 1970). Geothermal wells (Eichelberger & Koch, 1979; Nielson & Hulen, 1984) and Continental Scientific Drilling Project corehole VC-2B (Hulen & Gardner, 1989) penetrated the Proterozoic basement beneath the present-day Valles caldera. The depth to the Proterozoic basement beneath the caldera varies from ~1·5 km beneath the west side of the caldera to 5 km in the east (Goff *et al.*, 1989).

Proterozoic rocks exposed or intersected by drillholes within the Valles caldera are exclusively granitoid,

although metavolcanic rocks were penetrated by the Fenton Hill well, just outside the western caldera margin (Laughlin *et al.*, 1983), and amphibolites occur along with granitoids as lithic fragments in the Bandelier Tuff (Eichelberger & Koch, 1979). Metavolcanic and metasedimentary rocks are also exposed in uplifts around the borders of the Española basin. Some Proterozoic lithics from the Bandelier Tuff are partly melted, and the Otowi Member magma chamber was actively stoping country rock at the time of eruption (Eichelberger & Koch, 1979). Hence, these lithics are derived from near the zone of magma storage beneath the volcanic field, and represent crustal lithologies actually involved in magmatism. This point is considered later in the paper.

In summary, JMVF volcanism probably results from extension acting on the presumably weak lithosphere of the Jemez lineament, which itself is a localizing force on regional Cenozoic magmatism. Several components may contribute to magmatism: convecting asthenospheric mantle, Proterozoic oceanic lithosphere, and a wide variety of crustal lithologies. The mantle source regions of basalts in the Rio Grande rift and adjacent regions have been variously considered to lie in the lithosphere and/or convecting asthenosphere (Perry *et al.*, 1987; Leat *et al.*, 1988, 1989; Duncker *et al.*, 1991; Johnson & Beard, 1993; McMillan, 1998; Wolff *et al.*, 2000; Baldridge, 2004). Largely on the basis of trace element and isotopic signatures in the lavas, three or four chemical types of mantle source have been invoked: the convecting asthenosphere, similar to the source for modern mid-ocean ridge basalts (MORB) (Leat *et al.*, 1988, 1989; McMillan, 1998; McMillan *et al.*, 2000); Proterozoic lithosphere enriched by basaltic melt (McMillan, 1998; Baldridge, 2004); and lithosphere enriched by fluids from subducting slab(s) during the Proterozoic (Leat *et al.*, 1988, 1989; McMillan, 1998) and/or the Cenozoic, perhaps further modified by loss of large ion lithophile elements (LILE) in pre-magmatic fluids (Duncker *et al.*, 1991). Importantly, Johnson & Beard (1993) used Hf isotopes to show that the Proterozoic lithospheric mantle component in Rio Grande rift lavas originally melted in the spinel stability field and is therefore of probable oceanic origin. Although all investigators recognize a role for crustal melting in regional magmatism, there is no consensus on whether or not trace element and isotopic features of the most primitive basalts bear a significant crustal imprint. For example, the arc-similar signatures of northern Rio Grande rift tholeiitic lavas with LILE/HFSE (high field strength elements) ratios greater than those of typical MORB and ocean island basalts (OIB) have been variously ascribed to crustal contamination of asthenosphere-derived magma (Duncker *et al.*, 1991) or a source in subduction-modified mantle (McMillan, 1998).

ANALYTICAL METHODS

Major elements and selected trace elements were analyzed by X-ray fluorescence (XRF) at New Mexico Institute of Mining and Mineral Technology (NMIMT; procedures of Hallett & Kyle (1993)) and in the Geoanalytical Laboratory at Washington State University (WSU; procedures of Johnson *et al.* (1999)). Results from the two laboratories are comparable (Johnson *et al.*, 1999). All Keres, Polvadera Group and basement samples were additionally analyzed for trace elements by inductively coupled plasma mass spectrometry (ICP-MS) at WSU [see Knaack *et al.* (1994) for procedures]. Additional data (including Sr and Nd isotopes) on Santa Fe Group and some Cerros del Rio lavas and basement samples are taken from Gibson *et al.* (1993) and Duncker *et al.* (1991), although most of Duncker *et al.*'s Cerros del Rio samples have been reanalyzed at WSU. In most diagrams presented here, all available data are plotted. In cases where high precision is an issue, for example U/Nb ratios, only WSU data are plotted.

Sr, Nd and Pb isotopes on Keres Group samples, and Sr and Nd isotopes on Taos Range basement rocks, were analyzed at University of California Los Angeles (UCLA). Following dissolution, samples for Pb analysis were brought up in a HBr–HNO_3 solution. Teflon columns (500 μl) with 100–200 mesh AG1X-8 anion exchange resin were cleaned with H_2O, dilute HCl and HNO_3, then pre-treated with the HBr–HNO_3 solution, and the sample solution was loaded onto the columns and washed with further HBr–HNO_3. Pb was collected from the resin with H_2O. Otherwise, the procedures of Davidson *et al.* (1993) were followed.

Sr and Nd isotopes on Polvadera Group samples, and Pb isotopes on Taos range basement rocks and some Polvadera Group samples, were analyzed under the supervision of Dr Robert Creaser at the University of Alberta using standard dissolution and ion exchange procedures; isotope ratios were determined on a Micromass S54 thermal ionization mass spectrometry (TIMS) instrument. Sr and Nd ratios were corrected for mass-dependent fractionation by normalizing to $^{86}Sr/^{88}Sr = 0{\cdot}1194$ and $^{146}Nd/^{144}Nd = 0{\cdot}7219$, respectively. During the period of analysis, SRM 987 averaged $^{87}Sr/^{86}Sr = 0{\cdot}71027$ and the Shin Etsu Nd standard averaged $^{143}Nd/^{144}Nd = 0{\cdot}512046$. Measured Pb ratios were normalized to values for NBS981 of $^{206}Pb/^{204}Pb = 16{\cdot}9356$, $^{207}Pb/^{204}Pb = 15{\cdot}4891$ and $^{208}Pb/^{204}Pb = 36{\cdot}7006$.

Pb isotope ratio analysis of Cerros del Rio and Santa Fe Group lavas were performed at McMaster University. Samples with loss on ignition (LOI) values >2%, together with samples that were suspected of having undergone post-eruptive alteration (e.g. carbonation) and those that required multiple analysis because of high Fe contents,

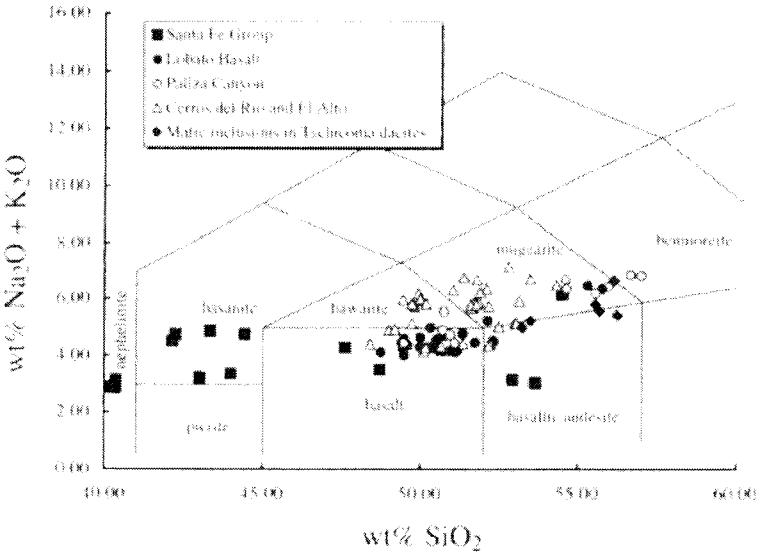

Fig. 2. Total alkali–silica classification diagram for JMVF mafic lavas. It should be noted that most are mildly alkaline in composition. In this and subsequent diagrams, data sources other than this study are Duncker *et al.* (1991) and Gibson *et al.* (1993); additional sources noted where relevant.

were leached in warm 6N HCl overnight and rinsed in quadruple-distilled water prior to digestion. Standard digestion techniques using HF, HNO_3, and HCl were employed. Pb was separated using standard anion exchange techniques using 0·7N HBr. Purified samples were then loaded on single Re filaments using silica gel, and analyzed on a VG 354 mass spectrometer using a single collector. During the period of analysis, NBS981 yielded mean values of $^{206}Pb/^{204}Pb$ = 16·901, $^{207}Pb/^{204}Pb$ = 15·447, and $^{208}Pb/^{204}Pb$ = 36·558 (n = 111). Data have been corrected for fractionation of 0·1% per a.m.u. In-run precisions of measured isotope ratios averaged ~0·06% (2σ). Total process blanks were less than 1 ng and are considered negligible. Pb isotopes on JMVF and Santa Fe range basement rocks were analyzed on a VG 54E mass spectrometer at Oxford University, using procedures similar to those at McMaster University.

Pb isotopes on Polvadera Group samples, and Sr, Nd and Pb isotopes on Bandelier Tuff basement lithics were separated using standard ion exchange procedures and analyzed using a ThermoFinnigan Neptune multicollector (MC)-ICP-MS at WSU. Pb procedures have been described by Wolff & Ramos (2003). Replicate isotopic analyses on selected samples indicate that the results from McMaster University, UCLA, University of Alberta, and WSU agree within error of the TIMS analyses; Pb isotope ratios analyzed by MC-ICP-MS are considerably more precise (Wolff & Ramos, 2003).

GENERAL CHARACTERISTICS OF JMVF MAFIC LAVAS

In this paper, we consider all lavas with <57% SiO_2 (nominally basalts and basaltic andesites). This cut-off is purely one of convenience; a complete continuum exists from the most mafic to the most silicic lavas in the JMVF. Many mafic lavas have alkaline affinities and are classified as hawaiites, mugearites and benmoreites (Fig. 2). Because geochemical groupings among JMVF mafic lavas (Fig. 3) were first recognized in the youngest flows (Duncker *et al.*, 1991; Wolff *et al.*, 2000), we describe the formations in order from youngest to oldest. Data are given in Table 1.

Cerros del Rio and El Alto fields

The Cerros del Rio mafic volcanic field occupies the south-central part of the Española basin. Our samples are mostly those of Duncker *et al.* (1991), for which we present new trace element and Pb isotope data. All come from the northern part of the field, within a ~15 km radius of White Rock (Fig. 1b). Lavas with <57% SiO_2 fall into two compositional groups: tholeiites, similar to the Miocene tholeiites, and nepheline- to weakly hypersthene-normative hawaiites/mugearites. The tholeiites were erupted between 2·48 and 2·33 Ma (Woldegabriel *et al.*, 1996), late in the history of the field, from vents located near its buried northwestern extremity east of the Rio Grande (Dethier, 1997).

Hawaiites and mugearites form a compositional continuum (Fig. 2). Olivine is the only phenocryst in the most

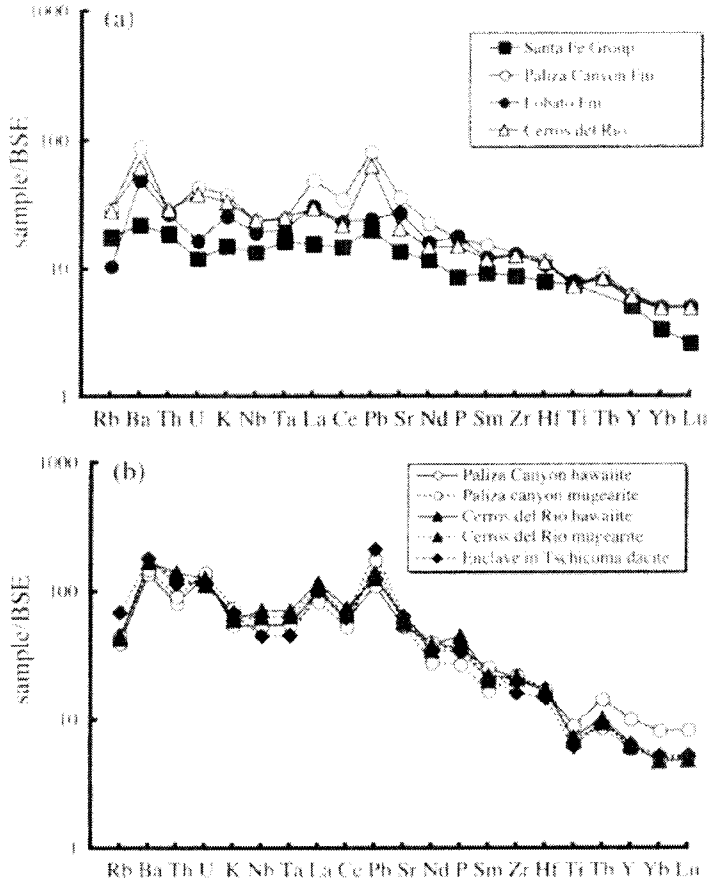

Fig. 3. Incompatible trace-element abundances in the scale JMVF mafic magma types, plotted by formation, normalized to Bulk Silicate Earth (BSE; McDonough & Sun, 1995). (a) representative andesites, (b) representative hawaiites (continuous lines) and mugearites (dotted lines). Despite overall similarity, mugearites tend to higher K/Nb and Pb/Ce ratios than hawaiites.

mafic hawaiites, but is joined by augite and hypersthene as silica increases. Quartz xenocrysts of crustal origin are common. These lavas dominate the White Rock Canyon sections sampled by Duncker *et al.* (1991) and most were erupted over a short time period (2·57–2·46 Ma, Woldegabriel *et al.*, 1996). They have distinctive incompatible trace element abundances, with approximately Bulk Silicate Earth (BSE) K/Nb and sub-BSE Rb/Nb, but elevated La/Nb and Th/Nb (Fig. 3b), and thus do not correspond to any common globally recognized mafic magma type (i.e. arc basalt, intraplate basalt, or MORB). Wolff *et al.* (2000) proposed that these compositions originated through mixing of nephelinite basanite, represented by the Santa Fe Group lavas (see below), with crustal melts.

Lavas and scoria of the much smaller El Alto field, in the northern JMVF, are petrographically and chemically similar to Cerros del Rio tholeiites, hawaiites and mugearites (Wolff *et al.*, 2000). This field may be slightly older than most of the Cerros del Rio lavas; one flow has been dated at 3·2 Ma (Baldridge *et al.*, 1980).

Polvadera Group

The Polvadera Group consists of the Lobato Basalt, Tschicoma, Puye, and El Rechuelos Rhyolite Formations (Bailey *et al.*, 1969). Of these, only the Lobato Basalt contains mafic lavas, although basaltic andesite and mugearite enclaves occur in some Tschicoma Formation dacites. The bulk of the Lobato Basalt was erupted between 10·8 and 7·8 Ma (Manley, 1982; Goff *et al.*, 1989), but flows interbedded with Santa Fe Group sediments in the northern JMVF, mapped as Lobato by Smith *et al.* (1970) and Aldrich & Dethier (1990), have been dated as old as 14·1 ± 0·3 Ma (Dethier *et al.*, 1986; Aldrich & Dethier, 1990). Most of our Lobato samples

Table 1: Major element, trace element and isotopic analyses of representative JMVF mafic lavas

Sample	JM93141	JM93-9A	JM93137	JM93176	JM93135A	JM93252	JM93198
Rock type:	nephelinite	tholeiite	mugearite	tholeiite	ol basalt	hawaiite	tholeiite
Formation:	SFG	SFG	SFG	PC	PC	PC	PC
SiO_2	40·32	48·88	54·47	49·44	50·67	50·71	50·91
TiO_2	2·18	1·47	1·86	1·67	1·84	1·83	1·47
Al_2O_3	10·72	16·98	15·57	18·14	16·00	17·76	15·48
Fe_2O_3	12·26	11·36	11·41	11·47	8·99	10·48	10·59
MnO	0·19	0·18	0·21	0·15	0·19	0·18	0·15
MgO	16·09	7·36	2·86	4·39	7·11	3·45	7·04
CaO	14·15	10·11	6·73	9·75	9·63	9·77	9·22
Na_2O	2·08	2·81	3·96	3·54	3·17	4·00	3·66
K_2O	0·80	0·74	2·23	0·96	1·77	1·58	1·12
P_2O_5	1·20	0·31	0·89	0·49	0·62	0·73	0·35
Trace elements analyzed by XRF							
Ni	421	94	112	82	79	31	101
Cr	552	180	229	58	248	40	238
Sc		33					
V		191					
Ba		370					
Rb	33	10	46	10	26	21	18
Sr	1291	651	719	1062	949	1107	808
Zr	243	126	616	147	202	219	143
Y	26	27	40	28	27	45	28
Nb	69	11	20	20	32	36	18
Ga	16	16	19	19	18	21	18
Co	82	57	32	69	96	58	58
Zn	93	89	142	86	71	100	81
Trace elements analyzed by ICP-MS							
La	77·84	16·23	53·16	37·59	51·69	65·41	32·51
Ce	148·30	31·72	101·50	70·07	93·54	101·71	59·75
Pr	17·84	3·86	11·68	8·38	10·17	12·48	7·18
Nd	71·08	16·65	50·12	33·82	40·36	50·63	29·06
Sm	14·41	4·26	11·37	7·04	7·97	10·42	6·46
Eu	4·05	1·54	4·27	2·20	2·27	2·89	1·96
Gd	10·25	4·59	10·09	5·66	6·50	9·48	6·01
Tb	1·30	0·78	1·46	0·93	0·97	1·44	0·91
Dy	6·11	4·84	7·96	5·30	5·51	8·48	5·35
Ho	0·99	1·01	1·47	1·05	1·03	1·67	1·06
Er	2·12	2·67	3·55	2·71	2·65	4·30	2·68
Tm	0·26	0·38	0·47	0·37	0·35	0·60	0·37
Yb	1·41	2·32	2·81	2·21	2·20	3·66	2·26
Lu	0·21	0·37	0·43	0·35	0·35	0·57	0·35
Ba	1043	346	1595	643	707	916	595
Th	10·51	1·68	6·14	2·53	5·65	8·42	2·30
Nb	72·70	9·31	29·57	18·96	33·20	35·72	15·95
Y	25·63	26·81	39·49	27·23	27·50	43·94	27·19
Hf	5·11	2·72	10·29	3·29	4·57	4·75	3·33
Ta	4·31	0·55	1·84	1·10	2·20	2·10	0·93
U	2·99	0·26	1·67	0·85	2·18	2·71	0·90
Pb	5·05	2·59	7·92	5·19	7·24	7·48	5·63
Rb	33·9	10·2	45·4	11·7	26·3	23·7	18·2
Cs	10·98	0·15	9·43	0·23	0·74	0·39	0·42
Sr	1250	651	696	988	893	1066	735
Sc	29·2	30·7	18·4	31·5	30·9	26·3	28·7
Isotope ratios							
$^{87}Sr/^{86}Sr$	0·70443		0·70538	0·70446	0·70430	0·70436	0·70446
$^{143}Nd/^{144}Nd$	0·51272		0·51256	0·51258	0·51261	0·51260	0·51244
$^{206}Pb/^{204}Pb$	18·928		17·629	17·369	17·804	18·269	17·200
$^{207}Pb/^{204}Pb$	15·529		15·514	15·533	15·507	15·472	15·450
$^{208}Pb/^{204}Pb$	38·846		37·394	37·272	37·609	37·709	36·325

Table 1: continued

Sample:	JM93232	JM9350-2	JM93233	JM9325	JM93262	JM93125	MR9047
Rock type:	mugearite	mugearite	mugearite	benmoreite	benmoreite	benmoreite	mugearite
Formation	PC	PC	PC	PC	PC	PC	Tsch. ME
SiO_2	54·56	55·51	54·59	56·61	55·92	58·95	53·48
TiO_2	1·47	1·48	1·42	1·19	1·43	1·34	1·20
Al_2O_3	18·61	18·04	18·28	17·30	18·14	17·31	18·04
Fe_2O_3	7·85	8·18	7·87	7·11	7·75	6·81	8·55
MnO	0·11	0·13	0·13	0·11	0·12	0·10	0·13
MgO	2·83	2·46	3·30	3·74	2·82	3·31	4·64
CaO	7·28	7·33	7·43	6·49	6·83	6·79	8·11
Na_2O	4·58	4·06	4·45	4·34	4·32	4·41	3·45
K_2O	2·16	2·18	1·94	2·54	2·16	2·45	1·80
P_2O_5	0·56	0·63	0·58	0·56	0·52	0·52	0·61
Trace elements analyzed by XRF							
Ni	20	43	15	49	21	32	28
Cr	17	29	64	36	29	55	39
Sc							19
V							192
Ba							1079
Rb	27	34	25	27	26	40	36
Sr	1197	1173	1219	1241	1025	945	1215
Zr	235	250	233	290	255	274	169
Y	27	54	27	27	29	25	27
Nb	36	38	35	35	36	40	32
Ga	19	19	21	20	20	19	21
Cu	41	55	39	31	36	25	83
Zn	69	75	65	69	73	49	85
Trace elements analyzed by ICP-MS							
La	54·48	81·32	54·90	74·05	54·17	59·45	50·99
Ce	89·55	103·33	88·87	121·13	87·52	96·57	95·56
Pr	9·30	13·28	9·36	13·38	9·17	9·81	10·73
Nd	34·91	52·07	35·36	49·73	35·18	36·58	40·71
Sm	6·86	9·88	6·92	9·05	6·81	6·85	7·86
Eu	2·06	2·66	2·06	2·43	2·03	2·04	2·31
Gd	5·69	9·23	5·82	6·87	5·96	5·77	6·46
Tb	0·87	1·36	0·89	0·99	0·89	0·86	0·93
Dy	4·94	7·92	5·05	5·36	5·14	4·84	5·19
Ho	0·97	1·64	0·99	1·02	1·01	0·96	1·01
Er	2·56	4·28	2·59	2·57	2·68	2·50	2·66
Tm	0·35	0·60	0·38	0·37	0·38	0·36	0·37
Yb	2·20	3·57	2·27	2·21	2·41	2·20	2·24
Lu	0·35	0·58	0·36	0·35	0·37	0·34	0·35
Ba	990	1068	1003	1455	981	1085	1045
Th	7·32	8·02	7·47	9·19	7·87	8·82	8·19
Nb	35·51	37·18	35·19	35·39	34·87	40·38	30·18
Y	25·83	50·29	25·90	26·37	27·35	25·25	26·10
Hf	4·91	5·25	5·04	6·48	5·14	6·77	3·99
Ta	2·03	2·14	2·04	2·15	2·04	2·44	1·66
U	2·88	3·33	2·98	3·25	2·91	3·48	2·08
Pb	11·86	12·82	12·17	16·70	12·77	13·00	13·32
Rb	27·6	35·1	24·2	27·6	27·5	40·5	37·6
Cs	0·27	0·75	0·68	0·59	0·65	0·71	1·53
Sr	1109	1071	1111	1180	979	896	1154
Sc	18·0	17·4	18·4	15·6	17·2	16·0	17·8
Isotope ratios							
$^{87}Sr/^{86}Sr$	0·70414	0·70422	0·70414	0·70477	0·70407	0·70431	
$^{143}Nd/^{144}Nd$	0·51262	0·51259	0·51263	0·51250	0·51262	0·51264	
$^{206}Pb/^{204}Pb$	18·108	18·062	18·099	17·771	18·062	18·080	
$^{207}Pb/^{204}Pb$	15·493	15·499	15·482	15·472	15·483	15·518	
$^{208}Pb/^{204}Pb$	37·946	37·906	37·957	37·541	37·894	37·985	

Table 1: continued

Sample	MR0013	MR0076	JW 001-1	JW 144-4	JW 144-10	JW 144-12	JW 144-16
Rock type	mugearite	benmoreite	tholeiite	tholeiite	ol basalt	bas and	alk basalt
Formation	Tsch. ME	Tsch. ME	Lobato SC	Lobato SC	Lobato SC	Lobato SC	Lobato SC
SiO_2	55·74	56·98	50·53	49·99	50·16	51·72	48·13
TiO_2	1·19	1·49	1·29	1·30	1·56	1·27	1·63
Al_2O_3	17·98	17·49	16·36	16·40	16·06	16·54	16·66
Fe_2O_3	7·63	7·81	10·87	10·93	10·87	10·61	11·74
MnO	0·11	0·15	0·16	0·16	0·16	0·14	0·17
MgO	3·49	2·96	7·33	7·47	7·38	6·18	5·74
CaO	6·74	5·74	9·04	9·33	8·72	8·75	11·42
Na_2O	4·12	4·33	3·40	3·40	3·54	3·54	3·35
K_2O	2·26	2·42	0·77	0·77	1·15	1·00	0·76
P_2O_5	0·73	0·63	0·26	0·26	0·40	0·25	0·40
Trace elements analyzed by XRF							
Ni	13	5	111	105	126	101	75
Cr	7	6	213	212	261	196	152
Sc	15	15	25	28	29	28	29
V	145	106	181	208	194	140	242
Ba	1297	1156	444	385	586	511	371
Rb	32	48	10	10	16	13	7
Sr	1252	641	512	513	662	539	604
Zr	228	227	118	115	143	115	144
Y	27	32	24	24	24	23	26
Nb	36	36	11	11	17	12	15
Ga	22	18	18	18	20	18	22
Cu	14	27	62	65	62	65	75
Zn	87	89	79	82	88	75	91
Trace elements analyzed by ICP-MS							
La	81·27	48·69	18·70	17·16	23·69	18·61	22·85
Ce	125·89	84·36	34·22	31·92	45·20	32·91	43·45
Pr	13·59	9·25	3·95	3·78	5·28	3·90	5·20
Nd	50·11	35·50	16·72	15·95	22·23	16·45	22·18
Sm	9·18	7·46	4·09	4·04	5·24	4·13	5·44
Eu	2·65	2·21	1·45	1·44	1·76	1·48	1·86
Gd	7·37	6·59	4·28	4·25	5·14	4·36	5·34
Tb	1·04	1·05	0·72	0·72	0·81	0·70	0·85
Dy	5·68	6·17	4·43	4·41	4·83	4·32	5·23
Ho	1·07	1·20	0·90	0·91	0·94	0·88	1·03
Er	2·69	3·16	2·49	2·45	2·50	2·37	2·74
Tm	0·38	0·44	0·36	0·35	0·35	0·34	0·38
Yb	2·28	2·75	2·16	2·14	2·12	2·08	2·29
Lu	0·35	0·43	0·34	0·33	0·33	0·32	0·35
Ba	1324	1252	467	386	561	489	354
Th	11·86	7·52	2·34	2·08	2·54	2·58	2·62
Nb	36·08	37·23	10·65	10·24	16·51	11·28	14·60
Y	29·79	32·10	23·86	23·67	24·60	23·22	26·82
Hf	5·30	4·93	2·85	2·67	3·35	2·81	3·24
Ta	2·10	2·26	0·68	0·62	0·99	0·71	0·84
U	2·77	2·07	0·74	0·65	0·79	0·82	0·43
Pb	15·21	12·17	5·69	4·94	5·08	6·09	3·94
Rb	33·9	47·7	12·5	10·8	16·5	13·3	7·50
Cs	1·12	1·39	0·36	0·35	0·42	0·22	0·02
Sr	1231	673	527	526	678	556	630
Sc	15·1	13·7	26·6	29·1	28·5	29·9	33·4
Isotope ratios							
$^{87}Sr/^{86}Sr$	0·70440	0·70414					
$^{143}Nd/^{144}Nd$	0·51259	0·51266					
$^{206}Pb/^{204}Pb$	17·916	17·604					
$^{207}Pb/^{204}Pb$	15·509	15·477					
$^{208}Pb/^{204}Pb$	37·772	37·451					

Table 1: continued

Sample:	JW 144/20	JW 238/1	MR 00/9	MR 00/7	SF-1	SF-9	O-1
Rock type	basalt	of basalt	of basalt	magnetite	hawaiite	hawaiite	hawaiite
Formation:	Lobato SC	Lobato	Lobato	Lobato	CdR	CdR	CdR
SiO_2	48.86	49.71	50.81	54.88	49.76	50.08	50.52
TiO_2	1.62	1.46	1.47	1.307	1.50	1.49	1.56
Al_2O_3	16.81	16.38	15.79	17.63	16.28	16.21	16.26
Fe_2O_3	11.85	10.97	9.79	8.76	9.82	9.72	9.57
MnO	0.16	0.19	0.15	0.12	0.15	0.15	0.15
MgO	5.34	6.57	7.17	3.90	6.98	6.89	6.55
CaO	10.93	10.09	9.63	8.34	8.70	8.78	8.83
Na_2O	3.25	3.41	3.54	4.36	4.25	4.04	4.06
K_2O	0.76	0.87	1.24	2.11	1.67	1.72	1.71
P_2O_5	0.38	0.36	0.41	0.69	0.89	0.93	0.78
Trace elements analyzed by XRF							
Ni	74	94	123	36	118	113	91
Cr	157	237	249	47	145	144	153
Sc	25	24	26	21	16	12	29
V	217	216	193	176	157	160	174
Ba	351	497	582	1639	1088	1152	1189
Rb	6	13	22	27	23	28	25
Sr	589	639	683	1240	1256	1315	1175
Zr	140	127	149	194	218	224	213
Y	27	29	22	23	26	26	25
Nb	16	20	25	24	44	46	42
Ga	20	19	17	21	18	18	20
Cu	75	79	62	43	57	53	48
Zn	88	85	80	76	83	84	83
Trace elements analyzed by ICP-MS							
La	20.56	27.13	29.54	59.12	72.61	78.50	63.86
Ce	39.94	44.95	53.51	97.38	119.34	128.82	106.66
Pr	4.79	5.45	6.11	10.34	12.37	13.32	11.33
Nd	20.85	22.84	24.77	38.86	46.34	49.55	43.40
Sm	5.09	5.31	5.57	7.23	8.59	9.12	8.43
Eu	1.72	1.74	1.85	2.19	2.63	2.75	2.57
Gd	5.15	5.42	5.32	5.90	6.94	7.23	6.81
Tb	0.82	0.86	0.83	0.84	0.98	1.03	0.97
Dy	4.88	5.18	4.77	4.81	5.43	5.49	5.46
Ho	0.99	1.04	0.94	0.91	1.02	1.04	1.01
Er	2.61	2.72	2.45	2.32	2.50	2.60	2.55
Tm	0.36	0.38	0.34	0.32	0.35	0.36	0.35
Yb	2.17	2.20	2.11	1.97	2.09	2.11	2.07
Lu	0.34	0.34	0.32	0.30	0.32	0.34	0.34
Ba	331	488	615	1654	1075	1162	1198
Th	2.17	2.68	3.56	7.14	10.91	11.49	8.71
Nb	13.02	18.54	26.87	25.82	45.78	47.46	44.35
Y	24.83	28.55	24.79	24.89	27.34	28.03	26.99
Hf	3.08	3.01	3.72	4.56	4.73	4.84	4.78
Ta	0.77	1.09	1.63	1.38	2.56	2.68	2.55
U	0.35	0.96	0.65	1.91	2.26	2.17	1.94
Pb	3.78	5.59	6.41	12.51	8.23	8.74	7.91
Rb	6.4	14.0	20.5	27.0	24.4	23.4	23.9
Cs	0.09	0.36	0.39	0.86	0.35	0.24	0.52
Sr	559	633	703	1249	1263	1322	1160
Sc	31.5	31.8	29.7	20.1	21.4	20.7	22.6
Isotope ratios							
$^{87}Sr/^{86}Sr$			0.70434	0.70466			
$^{143}Nd/^{144}Nd$			0.51273	0.51254			
$^{206}Pb/^{204}Pb$			18.059	17.847			
$^{207}Pb/^{204}Pb$			15.474	15.497			
$^{208}Pb/^{204}Pb$			37.772	37.613			

Table 1: continued

Sample:	PL	I-6	I-3	H-9	SF-3	I-5	WR-1
Rock type:	alk basalt	alk basalt	basalte	mugearite	mugearite	mugearite	tholeiite
Formation:	CdR	CdR	CdR	CdR	CdR	CdR	CdR
SiO_2	49·52	48·79	50·29	51·36	52·86	52·06	51·57
TiO_2	1·55	1·58	1·65	1·55	1·34	1·48	1·45
Al_2O_3	16·32	15·45	16·99	17·41	16·30	17·30	15·98
Fe_2O_3	10·52	13·13	9·78	9·34	10·28	9·00	11·07
MnO	0·15	0·16	0·15	0·13	0·16	0·13	0·16
MgO	6·39	5·57	5·56	5·22	4·85	4·50	5·79
CaO	9·70	9·40	8·86	7·84	8·61	7·91	9·34
Na_2O	3·49	3·51	4·24	4·37	3·75	4·63	3·35
K_2O	1·34	0·83	1·70	1·92	1·19	2·07	0·87
P_2O_5	0·64	0·48	0·78	0·86	0·64	0·92	0·32
Trace elements analyzed by XRF							
Ni	96	70	54	60	54	46	61
Cr	178	197	83	26	126	68	146
Sc	25	24	23	14	18	17	23
V	193	246	174	153	124	169	171
Ba	261	477	1022	1262	955	1213	443
Rb	18	12	21	24	11	29	16
Sr	875	539	1181	1215	776	1300	423
Zr	166	135	210	231	168	245	136
Y	25	24	25	26	25	27	25
Nb	31	21	42	45	30	49	17
Ga	19	19	19	23	21	19	21
Cu	42	66	46	37	50	50	68
Zn	86	106	88	82	87	85	91
Trace elements analyzed by ICP-MS							
La	49·30	25·03	59·92	70·32	48·97	75·47	19·69
Ce	83·72	46·98	102·34	114·16	83·83	122·51	37·47
Pr	8·99	5·70	10·89	12·25	8·96	12·66	4·37
Nd	34·63	24·12	41·82	45·68	34·24	47·23	19·11
Sm	6·89	5·62	8·11	8·73	6·98	8·85	4·88
Eu	2·17	1·85	2·49	2·63	2·07	2·64	1·68
Gd	6·10	5·37	6·58	6·95	5·99	6·98	5·14
Tb	0·90	0·85	0·96	1·00	0·88	1·00	0·84
Dy	5·10	5·03	5·27	5·56	5·01	5·61	5·05
Ho	0·95	0·96	1·01	1·09	0·96	1·04	1·00
Er	2·49	2·43	2·51	2·65	2·46	2·63	2·54
Tm	0·34	0·34	0·35	0·37	0·34	0·37	0·37
Yb	2·06	1·93	2·07	2·17	2·04	2·19	2·19
Lu	0·32	0·30	0·32	0·35	0·32	0·34	0·33
Ba	769	475	1015	1249	953	1203	414
Th	7·64	2·99	8·10	10·33	7·98	11·03	2·37
Nb	31·98	21·01	43·47	46·87	30·78	49·69	16·11
Y	25·46	25·11	26·88	28·51	25·56	28·20	26·13
Hf	3·73	3·21	4·63	5·01	3·93	5·34	3·22
Ta	1·87	1·28	2·43	2·67	1·92	2·88	0·96
U	1·37	0·89	1·85	1·65	1·18	2·03	0·70
Pb	5·69	2·77	7·59	8·76	7·11	9·75	4·35
Rb	18·3	12·6	21·6	23·8	10·9	29·1	17·5
Cs	0·41	0·09	0·30	0·12	0·18	0·30	0·43
Sr	912	563	1167	1220	808	1300	425
Sc	26·8	28·2	22·3	19·1	22·6	19·1	27·0
Isotope ratios							
$^{87}Sr/^{86}Sr$		0·70425			0·70429	0·70413	
$^{143}Nd/^{144}Nd$		0·51270			0·51269	0·51267	
$^{206}Pb/^{204}Pb$		18·223			18·083	18·305	
$^{207}Pb/^{204}Pb$		15·530			15·540	15·529	
$^{208}Pb/^{204}Pb$		38·096			37·963	38·129	

Table 1: continued

Sample	EA 3	EA 4	EA 6	EA 8	EA 9	EA 11
Rock type	tholeiite	mugearite	tholeiite	mugearite	mugearite	tholeiite
Formation	El Alto	El Alto	El Alto	El Alto	El Alto	El Alto
SiO_2	52·48	51·16	52·53	51·20	51·08	51·67
TiO_2	1·29	1·43	1·27	1·32	1·56	1·38
Al_2O_3	16·74	16·87	16·72	16·40	17·10	16·04
Fe_2O_3	9·66	9·57	9·66	9·53	9·77	10·29
MnO	0·14	0·14	0·14	0·14	0·14	0·15
MgO	5·77	6·12	5·66	5·76	5·71	5·93
CaO	8·43	8·31	8·52	8·92	8·24	8·78
Na_2O	3·59	4·21	3·63	4·24	4·38	3·52
K_2O	1·61	1·45	1·47	1·58	1·45	0·88
P_2O_5	0·39	0·74	0·39	0·92	0·67	0·36
Trace elements analyzed by XRF						
Ni	48	77	46	89	76	140
Cr	74	94	75	93	80	218
Sc	25	20	24	21	25	25
V	176	172	183	165	178	181
Ba	873	966	804	1406	1100	1356
Rb	22	15	23	21	17	15
Sr	626	1173	636	1347	1094	703
Zr	152	208	154	231	196	145
Y	24	24	23	25	24	25
Nb	22	35	22	39	31	15
Ga	19	21	16	18	20	17
Cu	25	26	24	12	22	33
Zn	78	85	76	84	87	86
Trace elements analyzed by ICP-MS						
La	33·09	61·60	31·33	75·97	53·51	31·44
Ce	54·59	104·12	54·60	128·34	87·55	51·29
Pr	6·38	10·87	6·24	13·35	9·37	6·08
Nd	25·09	41·16	24·66	50·02	36·08	25·49
Sm	5·67	8·05	5·54	9·07	7·28	5·84
Eu	1·81	2·50	1·77	2·81	2·31	1·87
Gd	5·27	6·55	5·11	7·07	6·02	5·63
Tb	0·82	0·95	0·79	1·03	0·89	0·84
Dy	4·90	5·17	4·70	5·40	4·95	4·95
Ho	0·99	0·98	0·95	1·02	0·97	1·00
Er	2·82	2·61	2·45	2·58	2·43	2·57
Tm	0·36	0·35	0·35	0·35	0·34	0·36
Yb	2·09	2·12	2·06	2·12	2·06	2·18
Lu	0·34	0·32	0·33	0·32	0·32	0·34
Ba	894	1006	769	1228	1054	1404
Th	2·78	6·67	2·85	9·41	5·78	2·79
Nb	21·24	33·67	21·64	37·80	30·09	13·66
Y	26·14	25·81	24·76	25·87	26·66	27·45
Hf	3·48	4·24	3·41	4·39	3·86	3·07
Ta	1·21	1·83	1·21	2·12	1·61	0·78
U	0·91	2·28	0·94	2·82	1·84	1·15
Pb	6·03	9·42	6·17	7·41	8·24	4·80
Rb	23·1	16·2	23·3	21·9	18·4	17·2
Cs	0·51	0·16	0·53	0·43	0·16	0·58
Sr	630	1193	649	1372	1111	717
Sc	25·1	19·8	24·7	18·5	20·0	27·3
Isotope ratios						
$^{87}Sr/^{86}Sr$						
$^{143}Nd/^{144}Nd$						
$^{206}Pb/^{204}Pb$						
$^{207}Pb/^{204}Pb$						
$^{208}Pb/^{204}Pb$						

XRF major and trace elements in JM93141, JM93137-2 and all Paliza Canyon samples analyzed at NMIMT; all other samples analyzed at WSU. All major element analyses are normalized to 100% volatile-free. All ICP-MS trace element analyses performed at WSU. Isotope laboratory details are given in the text. SFG, Santa Fe Group; PC, Paliza Canyon; SC, Santa Clara Peak section in Lobato Formation; Tsch. ME, mafic enclave in Tschicoma Formation dacite; CdR, Cerros del Rio.

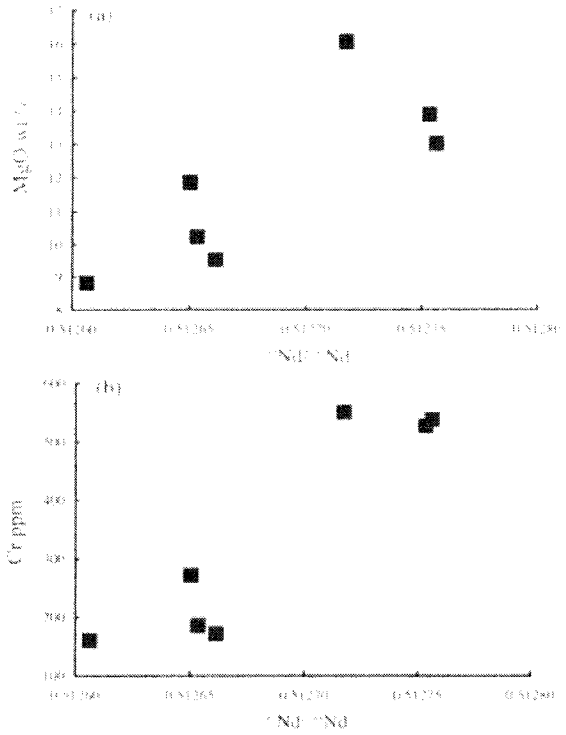

Fig. 4. $^{143}Nd/^{144}Nd$ vs (a) MgO, (b) Cr, in the Santa Fe Group primitive (basaltic andesite) lavas.

come from the Clara Peak shield section of Goff *et al.* (1989), and are tholeiites with a few weakly *ne*-normative lavas; this predominance of tholeiites is probably representative of the Lobato basalt as a whole (Goff *et al.*, 1989). Lobato tholeiites are olivine-phyric with sparse xenocrysts of quartz. MgO contents for the samples we have analyzed fall in the range 3·9–7·9%, and the lavas are generally compositionally similar to the later Cerros del Río and El Alto tholeiites (Figs 2 and 3a).

Mafic enclaves with ~53% SiO_2 in Tschicoma Fm dacite lavas (~7·2 Ma; Smith & Kudo, 1986; Goff *et al.*, 1989) are rounded to angular and typically 2–10 cm (maximum 50 cm) in size. Crenulate and sometimes diffuse margins indicate that they were at least partially liquid at the same time as the host dacite. Their alkali contents overlap with the Paliza Canyon mugearites and they are slightly less alkaline than the otherwise similar Cerros del Río mugearites (Fig. 2), but have the same distinctive trace element patterns as both these groups of lavas (Fig. 3b).

Paliza Canyon Formation

The Keres Group, which displays a spectrum of magma types from basalt to rhyolite, formed between 1·3 and 0 Ma, coincident with an episode of crustal extension in the adjacent Española basin (Gardner *et al.*, 1986). Following Goff *et al.* (1990), all Keres Group mafic lavas are assigned to the Paliza Canyon Formation.

The formation is dominated by andesite, with subordinate volumes of basalt and dacite flows. Mafic lavas include olivine tholeiites, olivine basalts, hawaiites, mugearites and benmoreites (Fig. 2) with MgO contents in the range 2·4–7·0% and fall into the same petrographic and trace-element groupings as the Cerros del Río lavas, although SiO_2 contents are slightly higher and all Paliza Canyon samples we have analyzed are at least weakly hypersthene-normative. Olivine tholeiites have subdued enrichments in incompatible trace elements and generally resemble tholeiites of other formations (Fig. 3a); one sample contains a quartzite fragment. Other basalts and hawaiites resemble the equivalent Cerros del Río lavas (Fig. 3b), although orthopyroxene is common in the mugearites and benmoreites; these lavas have the distinctive high La/Nb and Th/K ratios. Plagioclase phenocrysts (An_{70-90}) typically show complex zoning and are resorbed with reaction rims suggestive of varying degrees of magma mixing and hybridization.

Santa Fe Group lavas

The oldest lavas that crop out within the confines of the JMVF are thin mafic flows interbedded with Santa Fe Group sediments, found just below the base of the Keres Group in the area of St. Peter's Dome (Fig. 1; see also Goff *et al.*, 1990). At 25–16·5 Ma (Gardner *et al.*, 1986; Woldegabriel *et al.*, 2003), they represent infrequent activity heralding the main onset of JMVF magmatism by several million years. Among them is a larnite-normative nephelinite flow (sample JM93141 in Table 1), which, at 16% MgO, is the most primitive lava so far described from the Jemez Mountains. It has 15% olivine phenocrysts and microphenocrysts up to 1 mm in diameter, and trace clinopyroxene. Most of the olivine grains show euhedral outlines with tiling fork and re-entrant rich morphologies indicative of rapid crystallization. Core compositions of olivines are Fo_{89-90}, with most in a restricted range Fo_{89-90} (average $Fo_{89.5}$). Many grains have Cr-spinel and Cr-rich magnetite inclusions. The average olivine composition is close to equilibrium with the calculated groundmass [assuming magmatic $Fe^{2+}/(Fe^{2+}+Fe^{3+}) = 0·85$ in the liquid], but is forsterite poor compared with the calculated composition (Fo_{91}) in equilibrium with the whole rock. We conclude that some accumulation of olivine has occurred; the range of olivine compositions is satisfied by 11–13% MgO in the pristine magma, which would correspond to removal of 10–15% olivine from the analyzed bulk composition.

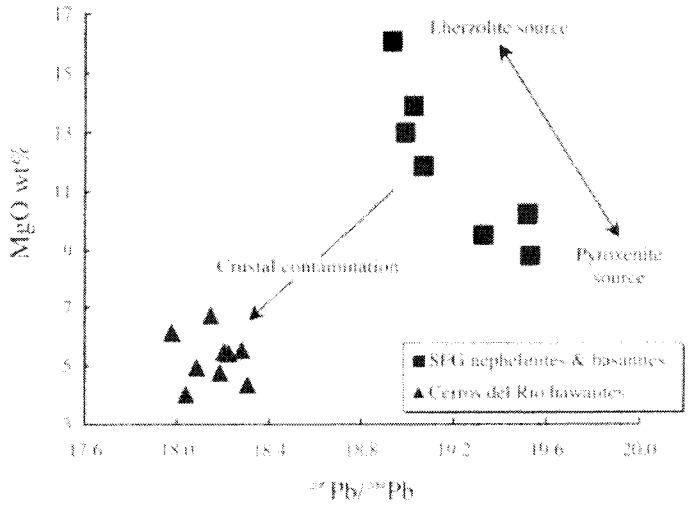

Fig. 5. $^{207}Pb/^{206}Pb$ vs MgO for primitive silica-undersaturated lavas and Cerros del Río basanites. Trend related to mantle source variability is distinct from that related to crustal contamination (see text).

The early St. Peter's Dome lavas, among which are intermediate compositions petrographically and chemically similar to Keres Group basaltic andesites and mugearites, form part of a more widespread, small-volume, early to middle Miocene volcanic episode in the Española basin (Gibson *et al.*, 1993) that includes tholeiites and quartz-normative basaltic andesites as well as basanites and nephelinites. The tholeiites and basaltic andesites have 2·9–7·1% MgO, trace element patterns resembling enriched MORB (E-MORB; Fig. 3a), and appear to have been only slightly modified by interaction with continental crust (Gibson *et al.*, 1993, and below); most resemble the younger tholeiites.

IDENTIFICATION AND ORIGIN OF JMVF PRIMARY MAGMAS

Nephelinite–basanite

The Española basin silica-undersaturated lavas were described by Gibson *et al.* (1993). Hereafter, we refer to these, and the St. Peter's Dome flows, collectively as 'Santa Fe Group lavas', consistent with the usage of Gardner *et al.* (1986) and Goff *et al.* (1990). They are of two types (Fig. 1): a more primitive group of nephelinites and basanites (MgO 13–16%; Ni 290–420 ppm; Cr 530–550 ppm; among which we place the St. Peter's Dome nephelinite), and a lower-MgO group of basanites and alkali basalts (MgO 9–12%; Ni 160–270 ppm; Cr 150–350 ppm). The latter have, on average, lower CaO, higher SiO_2, REE, Nb/Zr, $^{206}Pb/^{204}Pb$, $^{207}Pb/^{204}Pb$ and lower $^{143}Nd/^{144}Nd$ (Fig. 1), and appear to be derived from a more enriched source than the higher-MgO, more silica-undersaturated group. The generally more enriched character of this group could be due to crustal contamination; however, relationships between Pb isotope ratios and compatible element abundances are inconsistent with contamination, which in the JMVF acts to decrease $^{206}Pb/^{204}Pb$ and $^{207}Pb/^{204}Pb$ (see below). In particular, compositions that represent the contaminated equivalents of the nephelinites (Wolff *et al.*, 2000) have lower Pb isotope ratios at lower MgO contents (Fig. 5). Hence, it is more likely that the low-MgO primitive group is derived from a more enriched mantle source with higher U/Pb, Th/Pb and lower Sm/Nd than the high-MgO group.

Recently, mixed lherzolite–pyroxenite mantle has been invoked as a significant source for OIB (Hauri, 1996; Hirschmann & Stolper, 1996; Sigmarsson *et al.*, 1998; Lassiter *et al.*, 2000). Pyroxenite veins may make up a few percent of the upper mantle (Hirschmann & Stolper, 1996), although the lower solidus of pyroxenite compared with peridotite may cause it to yield a disproportionately high fraction of the total melt from a volume of veined mantle. Potential sources of pyroxenite include recycled lower-crustal cumulates, frozen melts, and subducted oceanic crust; the last may be especially significant in an ancient suture zone such as the Jemez lineament. Pyroxenite melts have higher SiO_2 and Al_2O_3, and lower CaO and MgO than small-degree melts of lherzolite. Some of the most compelling evidence for a pyroxenite contribution to mafic magma comes from primitive silica-undersaturated suites such as Hawaiian post-erosional lavas (Lassiter *et al.*, 2000), and the alkalic series of Grand Comore (Class *et al.*, 1998*b*, 1999; C. Class, unpublished data), in which major elements are correlated with Os

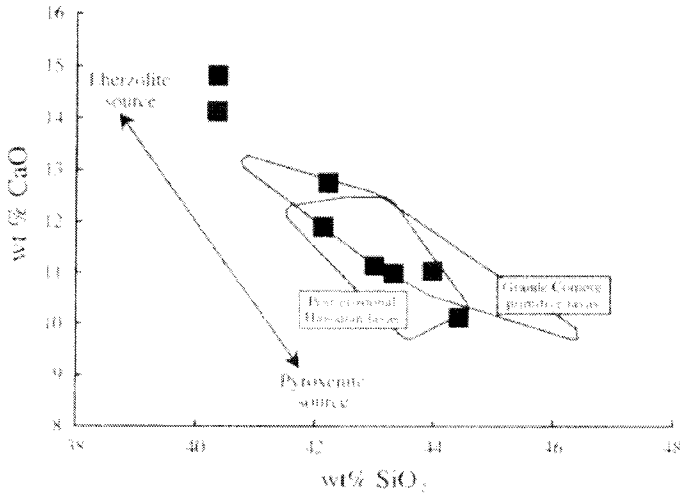

Fig. 6. CaO vs SiO_2 for suites of primitive Santa Fe Group (SFG) silica-undersaturated lavas. Data points are Santa Fe Group nephelinites and basanites; labeled fields are Hawaii and Grand Comore (see text). In each case, magmas containing a higher proportion of melt derived from pyroxenite are thought to be richer in SiO_2 and poorer in CaO. It should be noted that fractionation of either olivine or clinopyroxene would produce a positive trend on this plot. Additional data sources: Gardner *et al.* (1986), Class & Goldstein (1997); Class *et al.* (1998); Reimers & Nelson (1994).

isotope ratios. Both of these examples are located on young oceanic lithosphere, where the very high Re/Os of pyroxenite compared with peridotite results in measurable differences in $^{187}Os/^{188}Os$ after a short ingrowth period (~10 Myr), in contrast to Sr, Nd and Pb isotope ratios. The major element variations of the Santa Fe Group undersaturated lavas closely mimic both the Hawaiian and Grand Comore suites (Fig. 6). Although we have no Os isotope data, the much greater age of the Proterozoic sub-JMVF lithospheric mantle (a lithospheric mantle source for these lavas is justified below) than the oceanic lithosphere beneath Hawaii and the Comores allows measurably greater ingrowth of ^{143}Nd, ^{206}Pb and ^{208}Pb in the pyroxenite as compared with the lherzolite source (Figs. 4 and 5). One contrast between the Santa Fe Group lavas and the oceanic suites is that the pyroxenite-derived melts in the latter have lower, not higher, abundances of incompatible trace elements, as the consequence of a higher degree of partial melting of the pyroxenite (Lassiter *et al.*, 2000). We do not regard this as a serious obstacle to the applicability of the 'mixed-source' model in this case, for two reasons: (1) the isotopic data demonstrate that pyroxenite is substantially enriched in incompatible elements compared with the lherzolite source (Fig. 1); (2) the implicit assumption of pyroxenite–lherzolite melting under the same thermal conditions breaks down if the spatial scale of heterogeneity is at the kilometer scale or more, which is likely to be the case beneath the JMVF if the main pyroxenite reservoir is old Proterozoic oceanic crust (see below).

Normalized trace-element plots of Santa Fe Group nephelinites and basanites are shown in Fig. 7. To minimize the effects of minor fractional crystallization on incompatible trace element abundances, compositions have been corrected for minor olivine fractionation or accumulation. The more primitive group have been corrected to 12% MgO based on olivine–liquid relations in JM93-11, whereas the lower-MgO, CaO lavas were corrected (somewhat arbitrarily) to an average value of 10% MgO. In these plots, the order of elements from left to right reflects increasing compatibility during partial melting of a four-phase lherzolite (ol + opx + cpx + sp or gt; Sun, 1980; Thompson *et al.*, 1983). Overall, the patterns fan slightly from right to left (Fig. 7), as expected for different degrees of partial melting. The relative depletion in K for the primitive lavas of both groups is the most striking feature of the normalized patterns.

Depletions in K relative to comparably incompatible elements are common among intraplate alkaline lavas, both in the ocean basins and on the continents. Explanations for the K depletion fall into two groups: (1) prior selective K depletion of the mantle source; (2) K is retained during partial melting by a residual potassic mineral such as amphibole or phlogopite. In the first case, K loss occurs prior to magmatism and there is no implied constraint on the physical nature of the mantle source. Incorporation of ancient subducted oceanic crust, stripped of K by dehydration during subduction, into the intraplate magma mantle source is a possible mechanism (Weaver, 1991). A major objection to this model in the present case is the lack of similarity in the behaviors of

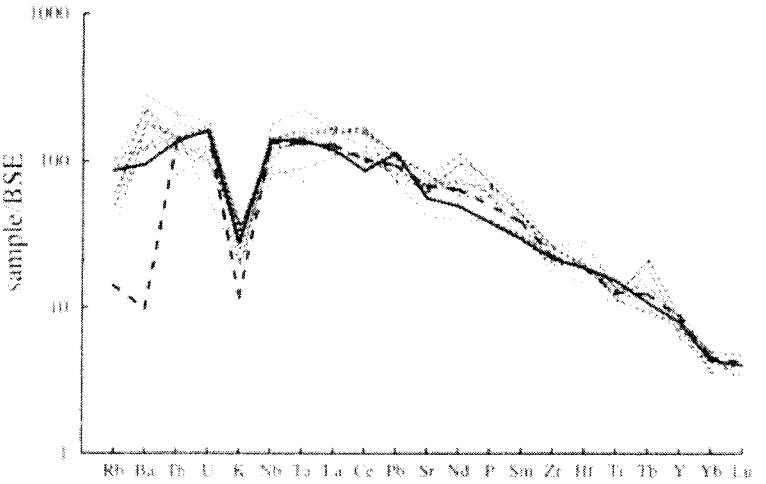

Fig. 7. Comparison of primitive silica-undersaturated JMVF lavas with results of mantle partial melting calculations involving residual hydrous phases. Thin dotted lines represent fractionation-corrected incompatible trace element abundances in primitive silica-undersaturated lavas, normalized to BSE of McDonough & Sun (1995), with Pb set to Pb/Ce = 0.04 (Sun & McDonough, 1989). Thick lines are fractional partial melting models for mantle with amphibole (continuous line) and phlogopite (dashed line). Model parameters: ol:opx:cpx:(amph or phlog) = 0.2:20:55:0.1, melt mode = 5:0:20:30:40:0, F = 1%. The models are insensitive to the proportions of olivine and pyroxene in the source for elements more incompatible than Nd. Mantle source was chosen to provide a fit to elements insensitive to the presence of hydrous phases, and consists of 40% depleted mantle, 40% primitive mantle, 10% normal MORB (N-MORB) and 10% E-MORB. Depleted mantle was calculated assuming that N-MORB of Sun & McDonough (1989) represents 20% batch melting of lherzolite (ol:opx:cpx = 0.6:32:8). MORB taken from Sun & McDonough (1989), and primitive mantle from McDonough & Sun (1995), with Pb set to Pb/Ce = 0.04. Neither model reproduces the relative Ti depletion, which may be due to inapplicable Ti distribution coefficients for amphibole or fractionation of spinel, or the relative Ba enrichment, which is a near ubiquitous feature of JMVF mafic magmas and hence may be a feature of the mantle source (compare the enriched source deduced for the Kenya Rift by Späth *et al.* (2001)). Sources of distribution coefficients: Hart & Dunn (1993); Hart *et al.* (1994); Johnson (1994); La Fourette *et al.* (1995); Dalpé & Baker (2000).

K and Ba (Fig. 7), which should be depleted to similar extents during slab dehydration and hence show coupled variation in lavas derived from sources with an ancient subducted component.

In the second case, the nature of the mantle source is constrained by the stability fields of amphibole and phlogopite in a lherzolitic assemblage. Primitive K-depleted basanites and nephelinites, very similar to the Santa Fe Group lavas, have been described from Grand Comore by Späth *et al.* (1996), Class & Goldstein (1997) and Class *et al.* (1998*a*), and from Kenya by Späth *et al.* (2001). In each area, those workers conclusively showed by careful modeling of cogenetic suites that melting of an anhydrous four-phase lherzolite source cannot account for the behavior of K, and that a hydrous K-bearing phase, more likely to be amphibole than phlogopite, must be present in the residue. The Santa Fe Group lavas were erupted at different times from widely separated locations and cannot be regarded as a cogenetic suite amenable to modeling as the products of a single partial melting event. None the less, we can show that the behavior of Ba, Rb and K are consistent with residual amphibole and allow a minor role, at most, for residual phlogopite. High-quality experimentally derived trace element partitioning data highlight the contrasting effects of phlogopite and amphibole on the compositions of liquids with which they equilibrate. Dalpé & Baker (2000) found that partition coefficients between amphibole and alkali basalt melt at mantle pressures (1·5–2·5 GPa) are several times higher for K than for Rb and Ba. In contrast, phlogopite–melt partition coefficients are similar for all three elements (La Fourette *et al.*, 1995). Rb and Ba are both less depleted and more variable than K in the undersaturated Santa Fe Group lavas (Fig. 7), consistent with amphibole being the dominant residual LILE-bearing phase rather than phlogopite. Illustrative results from partial melting calculations using assemblages with amphibole and phlogopite are shown in Fig. 7. We conclude that the most likely origin of these magmas is low-degree partial melting of amphibole-bearing mantle.

Amphibole is stable under the P–T conditions of the lithospheric mantle, but not in the convecting upper mantle or upwelling plumes (Class & Goldstein, 1997, and references cited therein). Therefore, the presence of amphibole in the mantle source region for the early Española basin nephelinites and basanites is evidence for melting of the subcontinental mantle lithosphere. Essentially the same magma type, modified by crustal contamination, appears to have been available for much of the lifetime of the JMVF (Wolff *et al.*, 2000, and below).

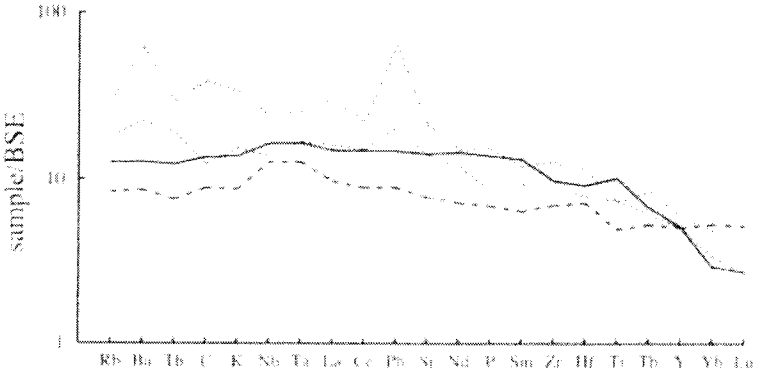

Fig. 8. Thin dotted lines show incompatible trace element abundances in tholeiites, normalized to BSE of McDonough & Sun (1995). Early tholeiite is the less enriched of the two; a Cerros del Rio tholeiite is the other (see also Fig. 3a). Thick continuous line is 8% partial melt of amphibole-free garnet lherzolite (mode otherwise as in Fig. 7). It should be noted that, both here and in Fig. 7, the models are insensitive to substitution of primitive mantle by depleted mantle + oceanic crust in the source; however, some crust is always required. Thick dashed line is E-MORB (cf. Sun & McDonough, 1989).

Hence, the mantle lithosphere appears to have been a major source of mafic magma during construction of the volcanic field. It should be noted that the K depletion is present in both groups of primitive undersaturated lavas. Therefore, we conclude that the nephelinite–basanite–alkali basalt magmas, which form an important parental magma type throughout the history of the JMVF, are derived from mixed lherzolite–pyroxenite–amphibole-bearing lithospheric mantle. Given the tectonic setting of the volcanic field, Proterozoic oceanic lithosphere associated with the Jemez lineament suture-zone is the likely source for these magmas. This conclusion is consistent with that of McMillan (1998), who invoked basalt-veined lithospheric mantle as the source for Espanola Basin lavas, and the Hf isotope evidence presented by Johnson & Beard (1993) for a component of ancient subvolcanic mantle in Cenozoic lavas of the Rio Grande rift and surrounding region.

Olivine tholeiite

Unlike the silica-undersaturated lavas, there are no primitive compositions among the *hy*-normative basalts, none have MgO >8 wt%, and all exhibit features consistent with at least minor crustal contamination. The latter is probably a consequence of lower incompatible trace element contents and hence sensitivity of the tholeiitic liquids to contamination, compared with the silica-undersaturated magmas. The Santa Fe Group basaltic andesites have higher $^{143}Nd/^{144}Nd$ (0·51280–0·51272) than Lobato and Cerros del Rio tholeiites (0·51273–0·51262) despite higher SiO_2 (Duncker *et al.*, 1991; Gibson *et al.*, 1993), and are less contaminated with crust. Abundances of compatible and incompatible trace elements are similar in tholeiites regardless of age. The normalized trace element patterns show mild depletions of Nb and Ta relative to LILE of similar compatibility (Figs 4a and 8), consistent with minor contamination, but lack the strong K depletion that characterizes the silica-undersaturated primitive magmas. We concur with Duncker *et al.* (1991) that the most likely parental basalt composition resembles E-MORB or tholeiitic OIB, similar to the MORB-like tholeiitic parent invoked by Dungan *et al.* (1986) as the mantle-derived component in the crustally contaminated Pliocene Servilleta lavas of the Taos Plateau (Fig. 1). This is consistent with the Sr and Nd isotopic composition of the least enriched of the early tholeiites ($^{87}Sr/^{86}Sr$ = 0·7038, $^{143}Nd/^{144}Nd$ = 0·51230, Gibson *et al.*, 1993), which lies within the E-MORB range. The convecting upper mantle is therefore a plausible source region for the parents of these magmas. None the less, the general Sr and Nd isotopic similarity to the silica-undersaturated magmas allows the parental magmas of the tholeiites to be partial melts of the same mantle, without residual amphibole (Fig. 8). Given the lower enrichments of incompatible elements in the tholeiites, this is most easily explained by a higher degree of partial melting with complete consumption of amphibole.

The relationship between the two primary magma types and their derivatives can be illustrated by consideration of critical trace element ratios. Using high-quality trace element data, Hofmann *et al.* (1986) showed that U/Nb and Pb/Ce ratios in ocean basin basalts, both MORB and OIB, exhibit little variation (U/Nb = 0·022 ± 0·005, Pb/Ce = 0·044 ± 0·009). Both ratios are much higher in average continental crust (U/Nb ~0·1, Pb/Ce ~0·25). The MORB and OIB values are considered representative of the convecting upper mantle. In Fig. 9, we have plotted U/Nb vs Pb/Ce (to avoid difficulties arising from

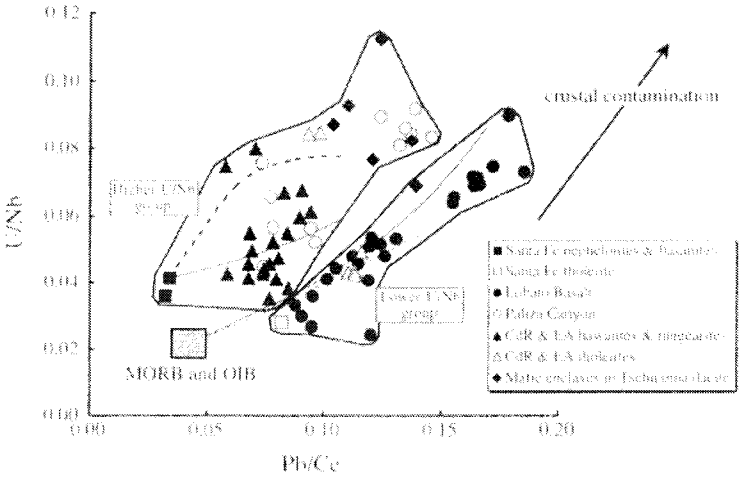

Fig. 9. U/Nb vs Pb/Ce for samples analyzed by ICP-MS at WSU. The majority of Lobato basalt samples define a low-U/Nb group, which also includes most Cerros del Rio (CdR) and El Alto (EA) tholeiites. MORB and OIB field is from Hofmann *et al.* (1986). Thin lines represent mixing of MORB (U 0.1 ppm, Nb 4.5 ppm, Ce 12 ppm, Pb 0.18 ppm) and mesh finite JM94H (Table 1) with average regional felsic crust; continuous lines and multi-crust dashed line, note that the two lines that have JM94H as the mantle-derived end-member are coincident. Mixing with MORB is terminated at 25% crust, mixing with JM94H is terminated at 50% crust. It should be noted that the Santa Fe Group and Lobato tholeiites with the lowest Pb/Ce (0.08–0.09) require less than 5% of the crustal component. Although the regional crust is in fact highly variable, the concave-upward feature arises from the higher concentrations of Pb in the crustal rocks, and is considered robust in simple mixing cases. However, partial melting of crust may yield highly variable trajectories in the diagram, illustrated by an EC-AFC simulation (heavy dashed line with JM94H as the starting magma (see Fig. 15 for model parameters).

inter-laboratory discrepancies, especially for U and Pb, only samples analyzed by ICP-MS at WSU are plotted). The data fall into two positively correlated arrays: a lower-U/Nb group defined by the Lobato Basalt, and a higher-U/Nb group dominated by the Paliza Canyon and Cerros del Rio El Alto hawaiites and mugearites. Most olivine tholeiites from Cerros del Rio and El Alto plot in the former group. Santa Fe Group nephelinites plot at the low-Pb/Ce, low-U/Nb end of the higher-U/Nb group, whereas a Santa Fe Group tholeiite bears the same relation to the low-U/Nb group. The increase in U/Nb and Pb/Ce among both groups is attributed to crustal contamination of mantle-derived magmas (this is justified in the next section), and examples of contamination trajectories are shown in Fig. 9. Also plotted is the limited MORB and OIB range (Hofmann *et al.*, 1986). Keeping in mind that crustal contamination has affected even the most primitive compositions among the Lobato lavas and Cerros del Rio El Alto tholeiites, MORB–OIB forms a plausible end-member for the lower-U/Nb array. A MORB–OIB end-member cannot satisfy the K–Th–Nb features of the high-U/Nb group, nor can the nephelinite basanite magmas for the low-U/Nb group (Wolff *et al.*, 2000), and below). The high U/Nb of the Santa Fe nephelinites is consistent with a role as parental magmas for the the Cerros del Rio hawaiites and Paliza Canyon lavas. The convergence of Cerros del Rio hawaiites and mugearites with Lobato basalts at low U/Nb suggests some mixing of components derived from both sources.

We have shown that the trace element abundances of the nephelinite basanite magmas are satisfied by low-degree partial melting of a MORB–OIB-like mantle source composition with residual amphibole (Fig. 7). The scatter among the high-U/Nb group in Fig. 9 may require a contribution from primitive magmas with still higher U/Nb than analyzed nephelinites, or may be the result of mixing with partial rather than bulk melts of crust, exemplified by the energy-constrained AFC curve shown in Fig. 9 (see below). The elevated U/Nb of the most primitive lava could be due to enrichment of the nephelinite basanite source with LILE prior to magmatism, although if this were due to metasomatism by a fluid, then elevated Pb/Ce might also be expected, yet Pb/Ce in the nephelinite basanite lavas is in the MORB–OIB range. Modeled partial melts for these magmas (Fig. 7) show an increase in U/Nb over primitive mantle, a consequence of significantly higher amphibole/melt partition coefficients for Nb than for U; Th/Nb is also elevated among this group. Therefore, the U/Nb–Pb/Ce relations are fully consistent with derivation from a MORB–OIB-like mantle source in the presence of residual amphibole. Hence, the contrasts between the two primary magmas (one silica undersaturated, one

tholeiitic can be attributed solely to the degree of melting and the consequent presence or absence of residual amphibole, which requires a lithospheric source for the nephelinite–basanite magmas. Although we cannot rule out an origin for the tholeiites in the convecting upper mantle, the simplest origin for the range of compositions among JMVF mafic magmas is therefore variable partial melting of amphibole-bearing lithospheric mantle with the incompatible element characteristics of asthenosphere, as modified by contamination with continental crust. Again, this is consistent with a source lying in ancient subducted oceanic lithosphere trapped in the regional suture zone beneath the JMVF.

These observations do not preclude an origin for the tholeiites in subduction-modified mantle (e.g. McMillan, 1998) with elevated levels of Pb and other strongly fluid-mobile elements. However, the extent of crustal contamination required to produce the entire range of Lobato Basalt and similar lavas (lower-U/Nb group, Fig. 9) is 25%, similar to the average amount of crust needed to produce the hawaiites from nephelinite–basanite magmas, and there is no reason to suppose a different crustal transport–residence history for the two groups of magmas.

To summarize, the two distinct groupings of JMVF mafic magmas, hawaiite–mugearite and tholeiite, are most simply explained as the respective products of strongly silica undersaturated and tholeiitic parents produced by different degrees of melting of lithospheric mantle and variably contaminated by continental crust. Crustal involvement increased dramatically with the tempo of magma production during the transition from scattered rift-related volcanism to the onset of construction of the JMVF, as a result of accumulation of heat in the crust with time. In the rest of the paper, we consider crustal lithologies and their interaction with the mantle-derived magmas.

EVALUATION OF CRUSTAL COMPONENTS IN JMVF MAGMAS

Although recognizing that not all crustal lithologies that interacted with mantle-derived JMVF magmas may be available at the surface, we have attempted to constrain possible contaminants by analyzing Proterozoic basement rocks from three areas (Fig. 1): the Taos range, ~100 km NE of the JMVF; eight samples of diverse lithologies around the Española basin (two amphibolites from the Santa Fe Range and two granites from west of the basin; and the Bandelier Tuff (four lithic fragments recovered from the Otowi Member). Our rationale for studying rocks from the Taos range is its position just north of the Jemez lineament combined with the southerly dip of the terrane boundary; hence formations exposed at the surface might have equivalents at depth beneath the JMVF.

Radiogenic isotope and trace element characteristics of regional crustal rocks

The basement lithologies fall into three broad categories: amphibolites (mafic–intermediate igneous protoliths); granitoid (silicic igneous protoliths), and metasediments. Sr, Nd and Pb isotope data for the basement rocks are compared with JMVF volcanics in Figs 10 and 11. Trace element and isotope characteristics are diverse, but we note the following features (Figs 10 and 11; Table 2).

(1) Almost all have LILE/Nb and Pb/Ce ratios well in excess of BSE values.

(2) Siliciclastic metasediment bears a highly distinctive imprint (elevated Zr and Hf) of detrital zircon.

(3) Lithologies represented by mafic amphibolites (Taos and Santa Fe ranges) that we have analyzed are eliminated as components in JMVF magmas by their Pb isotope characteristics.

(4) Lead isotope ratios in three basement fragments recovered from the Bandelier Tuff (two granitoids and an intermediate amphibolite), and a single granitoid from the Taos Range, are similar to the majority of JMVF silicic rocks and hence are candidates for crustal components in the magmas (Fig. 11). However, all four have highly radiogenic Sr, with $^{87}Sr/^{86}Sr$ >0·724.

How significant are the crustal components in JMVF magmas?

Previous geochemical studies of the JMVF (Singer & Kudo, 1986; Duncker *et al.*, 1991; Wolff *et al.*, 2000) have invoked a significant role for continental crust in JMVF magmas of nearly all compositions. In this section, as a preliminary to identifying the crustal components we briefly show that our much larger dataset supplies additional evidence for the presence of abundant crustally derived material.

Petrographic evidence

The Cerros del Rio hawaiites, mugearites and benmoreites contain unequivocal evidence for the presence of assimilated crust, in the form of rounded quartz xenocrysts, up to 2·5 mm in diameter, that have $\delta^{18}O$ values up to 3‰ higher than the host rock (Duncker *et al.*, 1991). Some of the quartz xenocrysts exhibit internal microcataclastic zones and oriented rutile needles, indicative of a metamorphic origin. The presence of large quartz grains requires assimilation of granitoid or metasedimentary rock. Quartz xenocrysts and quartzite fragments also occur in Paliza Canyon and Lobato basalts.

Geochemical evidence

All JMVF formations show positive correlations between LILE/Nb, Pb/Ce and indices of fractionation such as SiO$_2$ (Fig. 12), despite the inherent inability of the

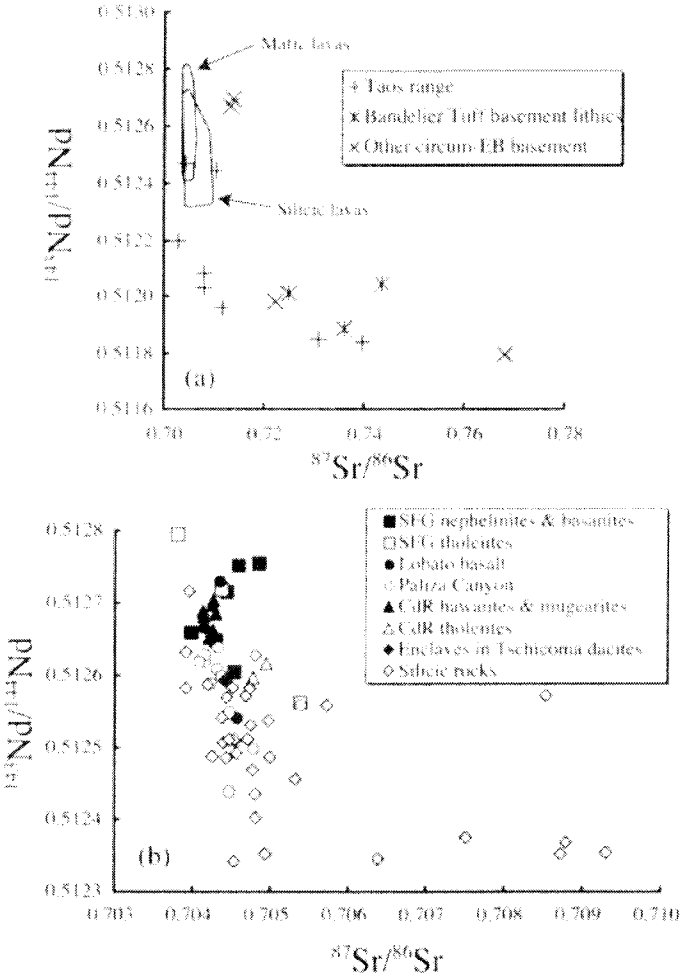

Fig. 10. (a) Nd–Sr isotope ratios of regional Proterozoic basement compared with JMVF pre-caldera volcanic rocks. (b) Detail of (a), showing JMVF rocks by formation and composition. Silicic rocks, shown for comparison, are all Keres and Polvadera Group samples with >57% SiO_2.

observed phenocryst assemblages (ol ± cpx ± opx ± plag ± Fe–Ti oxides) to induce significant fractionation of K and U from Nb, and of Pb from Ce. The correlation between K/Nb and SiO_2 extends smoothly from the Cerros del Rio and El Alto basanites/mugearites through Paliza Canyon into the silicic lavas of the Keres and Polvadera Groups (Fig. 12a); K/Nb ratios of basement rocks extend up to 10 000. Pb/Ce vs SiO_2 shows closely similar behavior (Fig. 12b); Pb/Ce ratios of basement rocks reach 1.69. K/Nb is negatively correlated with $^{143}Nd/^{144}Nd$, both overall and among individual formations (Fig. 13). We conclude that the LILE geochemistry of JMVF pre-caldera rocks, including andesites and more silicic compositions that are not treated in detail here, is dominated by crustal additions to mantle-derived magmas.

An alternative is that LILE-enriched subcontinental lithospheric mantle has contributed to elevated K/Nb in JMVF magmas. Such a contribution cannot be completely ruled out, but is unlikely for three reasons. First, available data from Colorado Plateau minettes (Alibert *et al.*, 1986), assumed to be products of such mantle, indicate a maximum Pb/Ce of 0.13, well below the maximum seen in JMVF mafic lavas, let alone the more silicic rocks (Figs 9 and 12b). Second, the complete continuum from mafic to silicic compositions with increasing K/Nb, Pb/Ce and decreasing $^{143}Nd/^{144}Nd$ (Figs 12 and 13) militates against the contaminant having a mafic composition. Third, potassic magmas erupted before or during the history of the JMVF are absent from the geological record of the Española Basin and vicinity (Gibson *et al.*, 1993),

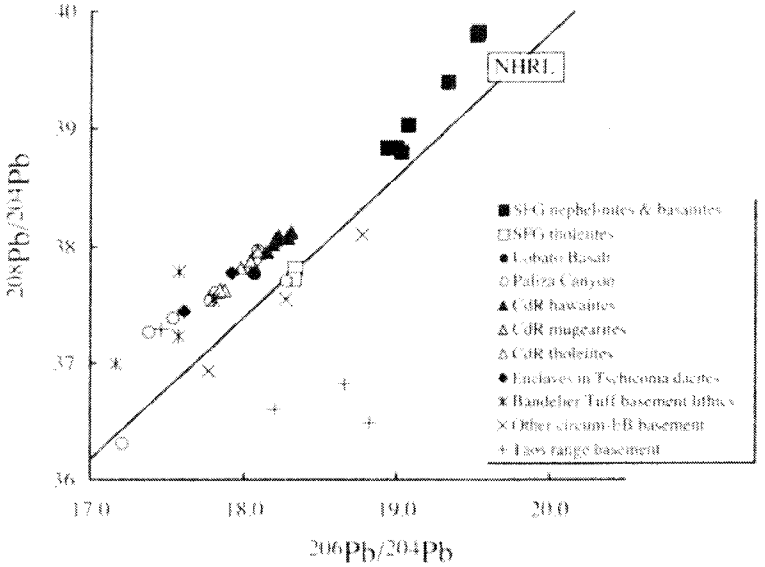

Fig. 11. $^{208}Pb/^{204}Pb$ vs. $^{206}Pb/^{204}Pb$ for JMVF pre-caldera mafic rocks, by formation, and regional Proterozoic basement samples. For clarity, only selected basement rocks are shown; the complete set of basement data is given in Table 2. NHRL, Northern Hemisphere Reference Line of Hart (1984).

suggesting that, if such mantle is present, it is not involved in magmatism.

Constraints on crustal components in JMVF magmas

Pb isotopes are especially useful for constraining crustal components, because: (1) the high Pb contents of crustal rocks gives them considerable leverage during mixing, hence the Pb isotopic compositions of contaminated lavas tend to be dominated by the crustal component; (2) straight mixing lines on Pb–Pb isotope ratio plots are an aid to interpretation. We first consider the interaction of the crust with Santa Fe Group undersaturated lavas, which have the most radiogenic Pb ratios of any in the JMVF: if they adequately represent the mantle component, then analyzed basement rocks with higher $^{206}Pb/^{204}Pb$ and $^{208}Pb/^{204}Pb$ (Table 2) can be eliminated as major contributors to the crustal component in JMVF magmas. Most of the mafic lavas lie on a linear array between the early undersaturated rocks and the four basement samples noted above (Fig. 11). The relationship is particularly clear among the weakly alkaline Cerros del Rio lavas, which show decreasing $^{206}Pb/^{204}Pb$ and $^{208}Pb/^{204}Pb$ with increasing degree of differentiation from basanite to mugearite. Pb isotope ratio–Pb/Ce–$^{87}Sr/^{86}Sr$ variations (see Figs. 15 and 16) also support the granitoid lithologies as plausible repositories for the crustal components in most JMVF mafic magmas. However, the isotope and trace element covariations are relatively insensitive to the mechanism by which component mixing occurs; this point is discussed in the next section. Whereas the granitoids are probably the dominant contaminants, a minor role for a siliciclastic metasediment component may be indicated by elevated Zr_N and Hf_N in the trace element patterns of some mugearites (Fig. 3b); the Sr, Pb and Nd contents of the metasediments are too low to make any significant impact on the isotopic composition of the mugearite (Table 2).

The tholeiites and their derivative magmas are more problematic, in part because we have found no uncontaminated primitive equivalents. Cerros del Rio tholeiites lie on the main Cerros del Rio–Paliza Canyon array in Pb–Pb space (Fig. 11), which probably reflects interaction with a the same type(s) of crust. The early rift quartz-normative lavas, which may be the least contaminated (Gibson *et al.*, 1993), lie on the Northern Hemisphere Reference Line (NHRL) of Hart (1984), along with a Paliza Canyon lava. The latter has $^{143}Nd/^{144}Nd$ = 0.51260 and elevated U/Nb and Pb/Ce, suggesting that it is contaminated, and that its position on the NHRL is fortuitous, as basement rocks that plot both above and below the NHRL are available as contaminants (Fig. 11). Another Paliza Canyon basalt flow that lies on the NHRL has the least radiogenic Pb of any rock sampled from the JMVF, with low $^{143}Nd/^{144}Nd$ and high Pb/Ce and U/Nb, and seems to require crustal contaminant(s) not represented among our basement

Table 2: Major element, trace element and isotopic analyses of Proterozoic basement rocks

Sample:	T161-2*	T163A*	T165A*	T176a*	T177*	T178*	LC1*
Rock type:	Granite gneiss	Amphibolite gneiss	Banded amphibolite	Metasediment	Amphibolite	Amphibolite	Garnet amphibolite
Area:	Taos Range	Taos Range	Taos Range	Taos Range	Taos Range	Taos Range	Taos Range
SiO_2	72·06	50·28	53·40	92·52	58·11	57·26	44·14
TiO_2	0·22	0·28	0·60	0·26	0·85	0·82	0·54
Al_2O_3	15·00	24·20	16·90	3·00	16·21	15·17	17·69
Fe_2O_3	2·19	5·13	8·56	12·64	10·93	11·62	16·29
MnO	0·03	0·08	0·17	0·01	0·21	0·18	0·23
MgO	0·78	4·18	5·17	0·02	2·80	3·46	8·92
CaO	1·96	12·90	9·65	0·10	4·33	5·77	9·68
Na_2O	4·11	2·63	4·41	0·85	4·90	5·25	1·89
K_2O	3·55	0·27	0·95	0·51	1·36	0·24	0·52
P_2O_5	0·10	0·06	0·20	0·01	0·29	0·24	0·09
Trace elements analyzed by XRF							
Ni	4	43	71	8	4	11	21
Cr							
V							
Rb	60	4	21	15	28	5	7
Sr	498	688	346	30	434	176	261
Y	6	5	20	2	25	19	34
Zr	95	13	55	514	78	60	75
Nb	5	3	5	4	7	6	11
Ga	19	18	14	8	18	16	22
Zn	50	49	78	15	168	97	124
Cu	31	7	379	7	22	88	52
Trace elements analyzed by ICP-MS							
La	33·1	4·6	7·5	1·4	17·2	12·3	10·2
Ce	69·6	7·9	14·7	2·4	34·7	24·8	29·6
Pr	6·07	0·99	1·97	0·24	4·23	3·11	4·46
Nd	19·05	3·91	9·29	0·81	18·45	13·94	21·16
Sm	2·60	1·01	2·75	0·14	4·52	3·46	6·91
Eu	0·51	0·61	0·95	0·13	1·49	1·02	1·80
Gd	1·71	1·05	3·20	0·14	4·42	3·45	6·68
Tb	0·21	0·16	0·54	0·03	0·69	0·55	1·06
Dy	1·05	1·08	3·48	0·18	4·29	3·25	6·13
Ho	0·20	0·22	0·72	0·05	0·88	0·68	1·25
Er	0·49	0·57	2·03	0·22	2·47	1·93	3·46
Tm	0·07	0·08	0·30	0·05	0·36	0·28	0·52
Yb	0·43	0·49	1·81	0·46	2·28	1·71	3·27
Lu	0·07	0·08	0·30	0·11	0·35	0·27	0·51
Ba	998	196	241	113	492	122	259
Th	12·4	0·2	0·9	12·3	2·0	1·4	1·2
Nb	3·6	0·8	2·5	1·9	5·3	4·1	5·8
Y	5·7	5·9	20·0	1·7	24·9	18·7	36·0
Hf	1·7	0·4	1·4	13·4	2·1	1·5	2·2
Ta	0·3	0·0	0·2	0·2	0·3	0·2	0·4
U	1·4	0·2	0·6	2·7	1·1	0·7	1·2
Pb	16·3	3·9	8·8	4·0	14·8	6·3	1·9
Rb	51·8	4·9	21·7	13·0	28·2	5·4	6·9
Cs	0·7	0·5	1·8	0·4	0·9	0·3	0·3
Sr	535	216	359	26	443	170	177
Sc	2·9	21·3	37·3	2·2	29·7	31·8	45·9
Isotopic ratios							
$^{87}Sr/^{86}Sr$	0·71163	0·70274	0·71039	0·73082	0·70802	0·70793	0·70424
$^{143}Nd/^{144}Nd$	0·51196	0·51220	0·51245	0·51185	0·51203	0·51208	0·51247
$^{206}Pb/^{204}Pb$	22·59	18·82	22·42	25·14	18·20	18·65	44·64
$^{207}Pb/^{204}Pb$	16·05	15·62	15·96	16·18	15·53	15·57	19·06
$^{208}Pb/^{204}Pb$	37·88	36·50	38·82	46·49	36·60	36·83	43·63

Table 2. continued

Sample	W10291*	RIN	PC 1	B4*	B8*	SdC 1A*	SdC 1B
Rock type	Granulite	Pelitic schist	Metarhyolite	Quartz monzonite	Granite	Amphibolite (leached)	Amphibolite (non-leached)
Area	Taos Range	Taos Range	Taos Range	Nacimiento Mountains	Jemez Mountains	Santa Fe Range	Santa Fe Range
SiO_2	70·62	66·23	81·32	66·41	74·48	53·24	
TiO_2	0·67	0·55	0·14	0·76	0·23	1·13	
Al_2O_3	15·18	27·48	12·11	15·32	13·98	14·32	
Fe_2O_3	6·94	4·24	1·28	4·83	1·50	12·63	
MnO	0·16	0·16	0·05	0·09	0·02	0·24	
MgO	1·74	0·15	0·10	1·54	0·39	6·05	
CaO	1·06	0·07	0·25	2·75	1·30	8·03	
Na_2O	1·43	0·27	0·87	3·32	2·96	3·32	
K_2O	2·05	0·75	3·87	4·73	5·09	0·87	
P_2O_5	0·14	0·10	0·02	0·25	0·06	0·18	
Trace elements analyzed by XRF							
Ni	20	22	5	16	8	34	
Cr		4	0				
V		6	6				
Rb	81	39	118	118	178	40	
Sr	185	102	62	375	166	191	
Y	29	204	50	43	19	33	
Zr	171	462	173	226	147	88	
Nb	12	39	21	10	10	8	
Ga	18	28	15	16	14	18	
Zn	65	73	44	75	38	117	
Cu	7	37	4	53	11	103	
Trace elements analyzed by ICP MS							
La	40·3	112·6	54·7	36·2	70·4	6·1	6·1
Ce	95·4	323·3	111·5	78·3	136·6	13·9	14·6
Pr	9·00	26·81	12·15	9·42	13·85	1·95	1·95
Nd	35·89	106·50	46·59	39·83	50·82	9·76	9·48
Sm	7·74	26·32	10·23	9·59	10·41	3·34	3·19
Eu	1·57	4·17	1·19	2·46	1·69	1·17	1·20
Gd	5·43	29·47	9·08	8·72	7·02	4·20	4·08
Tb	1·03	5·63	1·54	1·39	0·97	0·80	0·79
Dy	6·08	37·18	9·53	8·29	4·78	5·38	5·27
Ho	1·20	7·80	1·98	1·64	0·84	1·19	1·16
Er	3·27	21·48	5·55	4·39	2·64	3·30	3·23
Tm	0·48	3·20	0·86	0·60	0·25	0·49	0·48
Yb	3·12	20·21	5·54	3·46	1·28	3·05	2·98
Lu	0·51	3·12	0·87	0·52	0·22	0·46	0·46
Ba	603	486	1314	1314	746	71	76
Th	9·5	39·4	14·6	3·4	21·9	0·7	0·8
Nb	11·9	39·0	19·8	10·5	11·2	3·9	4·1
Y	31·2	206·7	51·5	44·2	22·0	31·0	30·9
Hf	4·4	14·8	6·1	7·9	5·4	2·4	2·2
Ta	0·9	3·2	1·5				
U	2·1	6·4	1·7	1·6	4·2	0·3	0·3
Pb	16·6	62·6	24·1	20·1	27·7	4·9	12·7
Rb	84·0	35·2	117·4	109·9	172·7	34·1	33·8
Cs	5·9	6·3	7·8	4·9	7·1	3·4	3·5
Sr	186	106	51	397	162	180	173
Sc	19·3	24·6	7·3	13·4	6·0	47·3	46·8
Isotope ratios							
$^{87}Sr/^{86}Sr$	0·73958			0·72216	0·76806	0·71362	0·71309
$^{143}Nd/^{144}Nd$	0·51184			0·51198	0·51180	0·51270	0·51267
$^{206}Pb/^{204}Pb$	17·46			17·76	18·77	18·27	19·41
$^{207}Pb/^{204}Pb$	15·51			15·52	15·62	15·55	15·70
$^{208}Pb/^{204}Pb$	37·29			36·94	38·11	37·55	38·79

Table 2: continued

Sample:	JM 18L-3	JM CCL-1	JM CCL-2	JM 18L-2
Rock type:	Granitoid lithic	Granite lithic	Amphibolite lithic	Amphibolite lithic
Area:	Bandelier Tuff	Bandelier Tuff	Bandelier Tuff	Bandelier Tuff
SiO_2	71·75	73·41	62·30	61·66
TiO_2	0·35	0·16	1·32	1·41
Al_2O_3	14·53	14·40	14·82	15·30
Fe_2O_3	2·31	1·04	8·02	9·12
MnO	0·03	0·02	0·15	0·12
MgO	0·72	0·51	3·24	2·35
CaO	1·79	1·45	2·53	3·50
Na_2O	3·97	4·11	3·91	3·77
K_2O	4·42	4·86	3·42	2·47
P_2O_5	0·13	0·05	0·29	0·31
Trace elements analyzed by XRF				
Ni	10	8	28	30
Cr	8	0	65	72
V	19	7	97	97
Rb	172	183	326	288
Sr	200	283	138	297
Y	25	19	48	53
Zr	230	73	449	491
Nb	16	8	21	19
Ga	19	17	23	25
Zn	44	33	324	229
Cu	6	19	36	10
Trace elements analyzed by ICP-MS				
La	26·1	21·2	86·0	72·7
Ce	50·4	40·1	165·1	141·7
Pr	5·49	4·31	18·41	15·93
Nd	21·45	16·21	73·82	64·91
Sm	4·79	3·51	15·14	13·68
Eu	1·68	1·04	3·19	2·91
Gd	4·66	3·07	13·14	12·12
Tb	0·79	0·49	1·90	1·80
Dy	5·14	2·90	10·70	10·38
Ho	1·08	0·56	2·01	1·99
Er	3·09	1·45	5·13	5·28
Tm	0·45	0·21	0·72	0·75
Yb	2·81	1·28	4·30	4·42
Lu	0·45	0·19	0·69	0·71
Ba	1279	1800	388	498
Th	5·1	5·8	14·1	15·3
Nb	16·4	4·0	17·4	16·1
Y	30·1	15·0	53·2	53·1
Hf	7·8	1·9	11·2	12·4
Ta	0·9	0·6	1·1	0·9
U	1·2	1·2	2·9	1·8
Pb	26·2	18·5	14·0	18·9
Rb	177·4	178·1	312·9	278·5
Cs	4·4	2·2	8·6	5·2
Sr	188	283	145	306
Sc	7·3	2·1	27·7	26·4
Isotope ratios				
$^{87}Sr/^{86}Sr$	0·74349	0·72484	0·73697	0·72187
$^{143}Nd/^{144}Nd$	0·51205	0·51201	0·51189	
$^{206}Pb/^{204}Pb$	17·163	17·568	17·795	17·572
$^{207}Pb/^{204}Pb$	15·433	15·472	15·489	15·471
$^{208}Pb/^{204}Pb$	36·998	37·235	37·548	37·786

*Major and trace elements analyzed by XRF at NMIMT; otherwise analyzed at WSU. All major element analyses have been normalized to 100% volatile-free. All ICP-MS trace element analyses were performed at WSU. Isotope laboratory details are given in the text. Amphibolite SDC-1, which contains calcite veins, was split into two aliquots for trace element and isotopic analysis; one aliquot (A) was leached in 2N HCl.

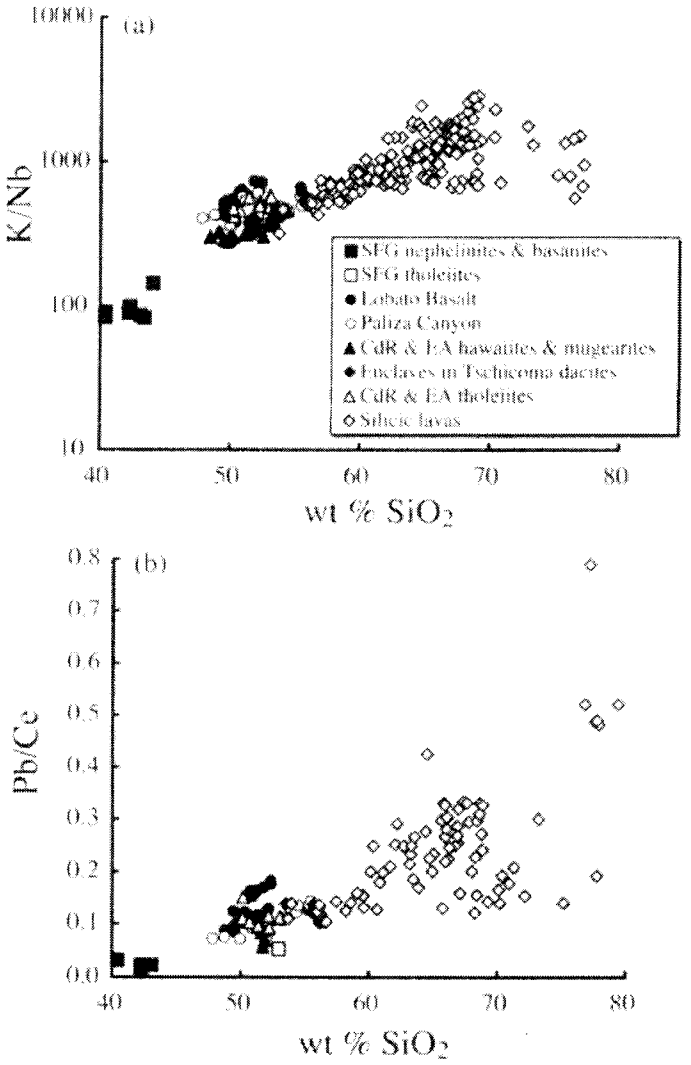

Fig. 12. (a) K/Nb and (b) Pb/Ce vs SiO_2 for all JMVF pre-caldera volcanic rocks. Note log scale for K/Nb. JMVF silicic rocks (hornorcites, andesites, dacites, rhyodacites and rhyolites) are shown for comparison.

samples (Fig. 14). However, both early rift lavas have much higher $^{143}Nd/^{144}Nd$, and one has low $^{87}Sr/^{86}Sr$ (Fig. 9b), consistent with negligible amounts of a crustal component.

The Sr (Pb, Nd) paradox

$^{87}Sr/^{86}Sr$ ratios in the JMVF mafic volcanic rocks fall within the relatively narrow range 0·7040–0·7048, despite a wide range in $^{143}Nd/^{144}Nd$ corresponding to 5 ε_{Nd} units in the mafic lavas and 9 ε_{Nd} units for all compositions (Fig. 10b), and the large variations in Pb isotope ratios. This is a fairly common feature of continental volcanic suites with a significant crustal component, and is seen elsewhere in the northern Rio Grande rift area (Dungan *et al.*, 1986; McMillan & Dungan, 1988). Usually, a crustal lithology with low time-integrated Rb/Sr and hence low $^{87}Sr/^{86}Sr$ is invoked as the contaminant, as Duncker *et al.* (1991) proposed for the Cerros del Rio lavas. This contaminant may be mafic crust with low Rb/Sr inherited from the protolith, and/or have lost Rb during high-grade metamorphism. Low-$^{87}Sr/^{86}Sr$ high-grade crust exists in the Taos range (Table 2), albeit with inappropriate Pb ratios for components in JMVF lavas. If Rb-depleted lithologies exist in the deep

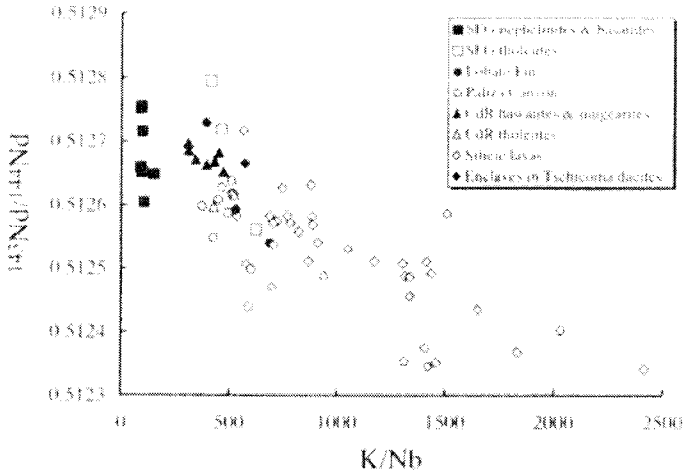

Fig. 13. K/Nb vs $^{143}Nd/^{144}Nd$ for JMVF pre-caldera rocks.

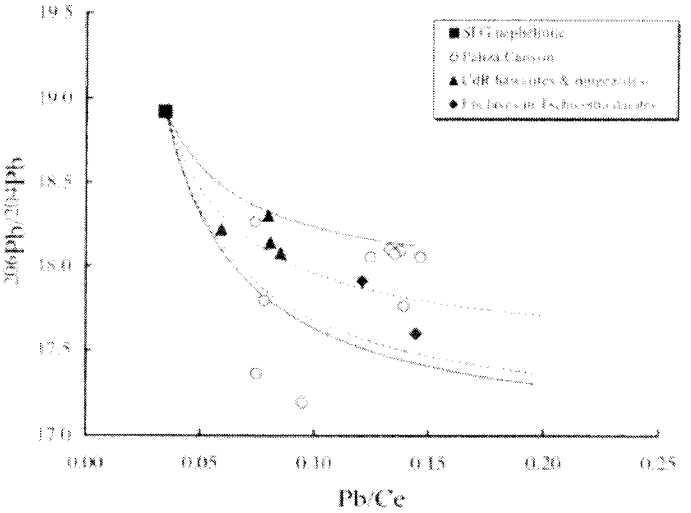

Fig. 14. Pb/Ce vs $^{206}Pb/^{204}Pb$ for JMVF pre-caldera mafic volcanic rocks. Dated curves represent simple mixing between Santa Fe Group nepheline JM9311 and two granitoid lithics from the Bandelier Tuff (JM 181-3 and JM CCL-1, Table 2). EC-AFC curves (see Fig. 15 for model input) do not differ significantly from the simple mixing line for each sample and are not shown. Continuous curves show simple mixing between Santa Fe Group nepheline JM9311 and two lavas representing extremes of Pb isotopic composition found among the silicic rocks (data from Rowe *et al.* (in preparation)), which may represent crustal compositions not found at the surface. The latter curves encompass all but two Paliza Canyon lavas with very low $^{206}Pb/^{204}Pb$, which cannot be modeled used any potential crustal end-member in our dataset.

crust beneath the JMVF, melts derived from them may be represented among the volcanic rocks by some of the dacite to rhyodacite lavas ($^{87}Sr/^{86}Sr$ = 0.7042–0.7053) of the Tschicoma Formation, which have closely similar Pb and Nd isotope ratios to the basement samples identified as likely contaminants. None the less, the presence of granitoids (some of which are xenoliths that have experienced partial melting; Eichelberger & Koch, 1979), that satisfy the Pb and Nd isotope requirements for the contaminant for all but two Paliza Canyon basalts, yet have high $^{87}Sr/^{86}Sr$ (Table 2), requires us to evaluate both analyzed upper crust and unseen lower crust as components. The granitoids are relatively Sr poor, and the amount of crustal Sr incorporated by the mafic magmas may be further restricted if assimilation proceeds by partial melting of granitoids, with plagioclase remaining in the residue.

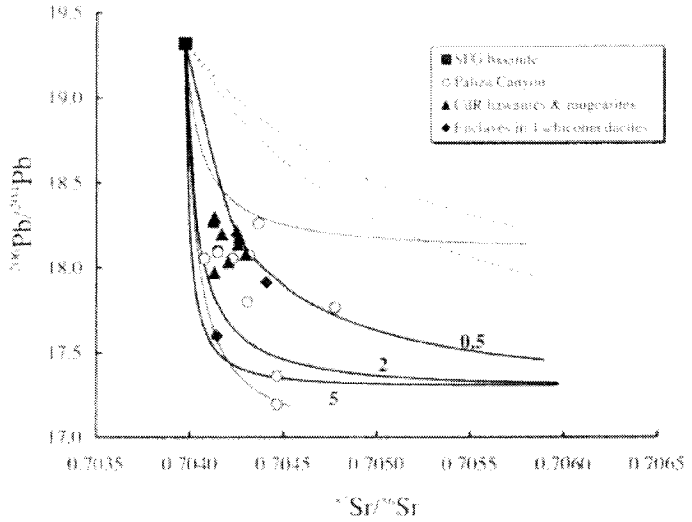

Fig. 15. $^{87}Sr/^{86}Sr$ vs. $^{206}Pb/^{204}Pb$ for JMVF primitive mafic lavas. Thin dotted and continuous curves are the same as in Fig. 14, except that Santa Fe Group basanite 89SB41 of Gibson *et al.* (1993) is used as the mantle-derived end-member. This sample has the least radiogenic Sr of the Santa Fe Group nepheline basanites, which span a similar range in $^{87}Sr/^{86}Sr$ to the JMVF lavas. Thick black curves are EC-AFC trajectories, labeled with the value of bulk D_{Sr} used for the assimilant and its partial melt. Assimilant is JM 10L-3 (Table 2). Most of the JMVF data fall between the EC-AFC curves for assimilant bulk D_{Sr} = 0.5 and 2; a value of five is considered unlikely, but is shown for illustration. It should be noted that this combination of end-members is the most favorable, but that assimilant D_{Sr} = 2 is required to encompass the majority of the data. Essentially identical results are obtained using a simple assimilant batch melting–magma mixing model with the same bulk D values (not shown). The simple mixing curves between the nepheline basanite and the two silicic lavas also encompass the JMVF data. Other EC-AFC chemical parameters used here and in Figs 13 and 17: magma bulk D values, Sr 0.2, Pb 0.05, Nd 0.07, Ce 0.15; assimilant bulk D values, Pb 0.15, Nd 0.15, Ce 0.2. Thermal parameters derived from MELTS: magma initial temperature = liquidus temperature = 1280°C; assimilant liquidus = 950°C; assimilant initial temperature = solidus = 800°C; C_p magma = 1.04 J/kg per K; C_p assimilant = 1.08 J/kg per K; H_{crys} = 396 kJ/kg; H_{fusion} = 554 kJ/kg. The high initial assimilant temperature is justified on the basis of geophysical evidence for high temperatures beneath the Rio Grande rift (Baldridge *et al.*, 1983; Clarkson & Reiter, 1983; Morgan & Golombek, 1984).

The EC-AFC numerical model of Bohrson & Spera (2001) and Spera & Bohrson (2001) provides a means of evaluating the assimilation of partial melts of crustal rocks into mantle-derived magmas. The model applies energy conservation (EC), based on the thermodynamic properties of magma and assimilant, to the assimilation–fractional crystallization (AFC) approach of Taylor (1980) and DePaolo (1981). A feature of the model is that anatectic melt produced as the country rock assimilant is heated above its solidus by the magma is immediately added to and homogenized with the magma body (Spera & Bohrson, 2001). Hence, the initial effects of assimilation are dominated by residue–melt partitioning in the country rock, particularly so as the anatectic melt is assumed to be fully extracted after each melting increment. For model input, we have calculated liquids and other thermodynamic parameters from MELTS (Ghiorso & Sack, 1995); input data for simulations are given in Fig. 15. For ratios between elements that are incompatible during assimilant melting (e.g. Pb, Ce, Nd), the EC-AFC curve is indistinguishable from a simple mixing curve corresponding to complete melting of the assimilant followed by magma mixing, but the two models diverge sharply for compatible elements such as Sr in the presence of residual plagioclase. Simple mixing between Santa Fe Group primitive magmas and granitoids cannot reproduce the Pb–Sr relations among JMVF mafic lavas (Fig. 15). In contrast, most of the lavas can be satisfactorily modeled by EC-AFC with variable compatible to mildly incompatible behavior of Sr during melting of the crust, using the most favorable combination of mantle and crustal end-members (Fig. 15).

Also shown in Fig. 15 are mixing lines between mantle-derived magma and two dacites that may represent melts of possible low-$^{87}Sr/^{86}Sr$, non-radiogenic Pb, and low-$^{143}Nd/^{144}Nd$ crust present at depth beneath the volcanic field. It is clear that these mixing lines also encompass the JMVF mafic lava data, in fact rather more inclusively than the EC-AFC models. $^{87}Sr/^{86}Sr$ covers a wide range (0.7039–0.7093) among Keres and Polvadera dacites and rhyolites, representing multiple sources, and can be used to support both lower- and upper-crustal sources of contamination. Petrogenesis of the intermediate and silicic JMVF rocks will be considered in a forthcoming paper (Rowe *et al.*, in preparation). The main point is that the isotopic data alone cannot distinguish

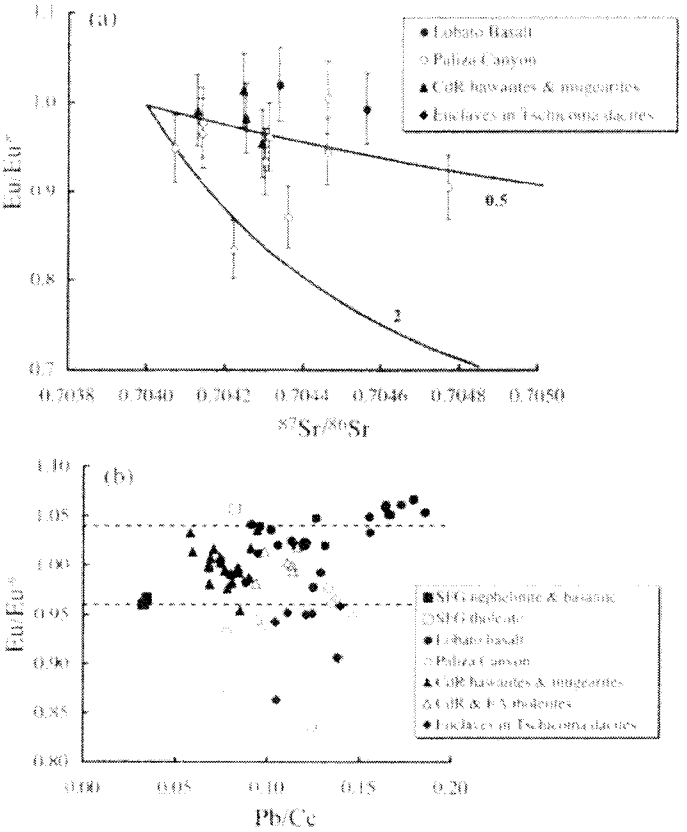

Fig. 16. (a) Eu/Eu* vs $^{87}Sr/^{86}Sr$ for JMVF mafic rocks. Curves are EC-AFC trajectories labeled with values of assimilant bulk D_{Eu}; other parameters are as Fig. 14. In both cases $D_{Eu} = D_{Sr}$. Error bars for Eu/Eu* indicate precision based on replicate analyses. (b) Eu/Eu* vs Pb/Ce for JMVF mafic rocks. Dashed lines show estimated analytical error of ±4% on Eu/Eu* = 1.

between mixing of mantle-derived magmas with low-$^{87}Sr/^{86}Sr$ melts derived from (presumably) lower crust, and partial melting of high-$^{87}Sr/^{86}Sr$ upper crust with Sr retained in residual plagioclase in the genesis of the JMVF mafic magmas.

Because Eu and Sr are geochemically similar, a significant role for residual plagioclase, or any other phase that sequesters Sr, in petrogenesis should result in the development of negative Eu anomalies in the REE patterns of the lavas. The majority of JMVF lavas, including andesites and dacites, do not show marked Eu anomalies. Within the limitations of the calculated Eu/Eu* values, EC-AFC does not model Eu anomaly development as accurately as it does Sr–Pb variations (Fig. 16a). More generally, few analyzed mafic lavas show measurable Eu anomalies (Fig. 16b). We conclude that although the upper crust/residual plagioclase contamination model can account for the geochemistry of some of the JMVF lavas, it is not a unique explanation and there must be some role for low-$^{87}Sr/^{86}Sr$ crust.

Ellison *et al.* (1996) considered $^{143}Nd/^{144}Nd$ vs $^{206}Pb/^{204}Pb$ variations in Keres Group lavas and suggested, on the basis of limited data for basement rocks, that both felsic and mafic lower crust were involved in petrogenesis. A re-examination of this plot in the light of our expanded dataset (Fig. 17) shows that simple mixing between JM93141 nephelinite and silicic compositions can satisfy the Nd and Pb isotopic compositions of nearly all the mafic lavas; it should be noted that these two isotopic systems are insensitive to the effect of residual plagioclase.

SUMMARY OF MAIN GEOCHEMICAL FEATURES OF MAFIC LAVAS, AND ORIGIN OF THE JMVF

The two parental magma types give rise to two distinct lineages of mafic lavas, the trace element signatures of which are shown in Fig. 3. Compared with BSE,

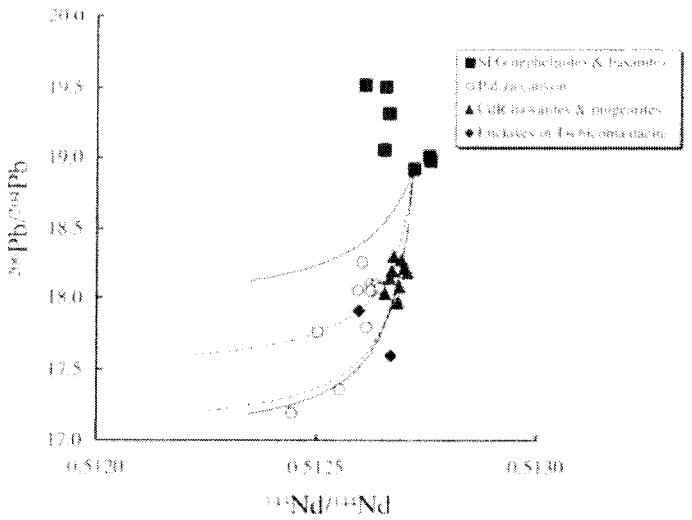

Fig. 17. $^{143}Nd/^{144}Nd$ vs. $^{206}Pb/^{204}Pb$ for JMVF pre-caldera lavas and selected basement rocks. Dotted and continuous curves are simple mixing lines, as in Fig. 11. EC-AFC trajectories do not differ significantly from mixing lines and are not shown.

tholeiites and their derivatives have variably elevated K/Nb and La/Nb as a consequence of crustal contamination. The same ratios are elevated in the hawaiites and several Paliza Canyon lavas when compared with their silica-undersaturated primitive parents, but because the latter are K-depleted, the effect of contamination has been to raise K_N to similar values to Nb_N and La_N, whereas other LILE/Nb ratios are significantly greater than BSE (i.e. the normalized pattern has a K–Nb–Ta trough; Fig. 3). This is the signature of the Rio Grande rift 'Type 3' magmas of Leat *et al.* (1988, 1989, 1990), which does not conform to any globally common magma type. Leat *et al.* (1988, 1989, 1990) also identified OIB-like magmas derived from the asthenosphere and potassic magmas derived from enriched continental lithospheric mantle. They proposed that the 'Type 3' lavas were derived from modified subduction-related mantle, ultimately related to shallow subduction of the Farallon plate beneath the region during the Mesozoic to early Cenozoic. Duncker *et al.* (1991) similarly interpreted the geochemistry of the Cerros del Rio hawaiites, and suggested that the 'Type 3' mantle was produced by conversion of phlogopite to amphibole during mantle shallowing consequent upon lithospheric extension, with loss of K in pre-magmatic fluids. Subsequently, Wolff *et al.* (2000) argued instead that the 'Type 3' compositions are the result of contamination of K-depleted silica-undersaturated liquids by continental crust, for which we have presented additional evidence. Based on the similarity of the nephelinite–basanite magmas to those erupted on oceanic islands, Wolff *et al.* placed their source in the asthenosphere. We have shown here that the affinity of the nephelinite–basanite lavas is more likely to be with OIB derived from the oceanic lithosphere (Class *et al.*, 1998*a*), generally consistent with independent evidence for the presence of ancient sub-oceanic mantle beneath the region (Johnson & Beard, 1993; McMillan, 1998), also concluded that lithospheric mantle, enriched with frozen basaltic melt, is a plausible source for the Espanola Basin mafic magmas.

Other volcanic fields along the northeastern Jemez Lineament [summarized by Dungan *et al.* (1989)] show the 'Type 3' signature. Both the Ocate and Raton–Clayton volcanic fields, NE of the JMVF, have mafic lavas with $K_N \sim Nb_N < La_N$. The Raton–Clayton 'Capulin Type' lavas are Type 3, with very high Th/K and Th/Nb. In addition, the Raton–Clayton field contains K-depleted basanites and nephelinites similar to, and in some cases even more undersaturated than, those of the Santa Fe Group, and we suggest that they are derived from the same belt of lithospheric mantle associated with the Jemez Lineament. Tholeiites with similar trace element characteristics to those in the JMVF also occur in both the Ocate and Raton–Clayton fields.

Leat *et al.* (1988, 1989, 1990) initially identified the 'Type 3' signature among lavas of the Flat Tops, Yarmony Mountain, and other volcanic fields of NW Colorado at the northern extremity of the Rio Grande rift. These fields form a NE–SW alignment that runs parallel to the nearby Colorado Mineral Belt and the Jemez lineament. Like the Jemez lineament, the Colorado Mineral belt marks a Proterozoic lithospheric discontinuity that has been reactivated during the Cenozoic [see Karlstrom *et al.* (2002) and references cited therein]. We suggest that the NW Colorado 'Type

'T' magmas of Leat *et al.* (1988, 1989, 1990) arise through essentially the same mechanism as that proposed here for the JMVF and Española basin, and that their parents are similar to the Santa Fe Group nephelinites and basanites, derived from similar lithospheric mantle sources of similar origin, i.e. Proterozoic oceanic lithosphere.

The contaminated, low-K Nb–Ta 'Type 3' liquids are an important magma type in the JMVF; among their derivatives are the volumetrically dominant Paliza Canyon andesites, and mafic enclaves in Polvadera group dacite lavas. Hence, they are likely to have been the main heat source for crustal melting and assimilation, with the tholeiites playing a subordinate role, implying that the lithosphere has been the dominant mantle source for mafic magma since the inception of the JMVF. There is no regional geographical age progression of volcanism in the southwestern USA, and the fundamental cause of JMVF magmatism is likely to be the action of lithospheric extension upon underlying fertile mantle, without any role for a deep-seated mantle thermal plume. This is supported by coincidence of individual volcanic and extensional episodes since the early Miocene (Self *et al.*, 1996; Gibson *et al.*, 1993). Melting of ancient oceanic lithosphere associated with the Jemez lineament suture may have been directly induced by extensional shearing and decompression at the intersection of the lineament with the Rio Grande rift, although heating by melts rising from the underlying up-arched asthenosphere may also have played a role. The inherently fertile character of the lithosphere beneath the suture is shown by the Jemez lineament alignment of volcanic fields and is consistent with geophysical evidence (Duecker *et al.*, 2001). The JMVF is by far the largest of the Jemez lineament volcanic fields, which we ascribe directly to the effect of Rio Grande rift extension on sub-lineament mantle.

ACKNOWLEDGEMENTS

This paper represents a partial summary of several years' work in the Jemez Mountains, to which many have contributed in tangible and intangible ways. We wish to thank Alan Dickin, Steve Self, Fraser Goff, Philip Kyle, Conny Class, Terry Spell, Scott Baldridge, Jon Davidson, Phil Leat, Bob Thompson, Mike Dungan, Stephen Moorbath, Anita Grunder, Rob Creaser, Jack Flannery, Katherine Romanak (née Duncker), Bruce Turbeville, Steve Balsley, Dave Kuentz, Marty Horn, Wade Anhin, Lee Winters and Pam Harrman for discussion, data, and/or assistance in field and laboratory. Jane Pedrick supplied many of the basement samples, and her help with the Precambrian geology was invaluable. Needless to say, none of the above-mentioned individuals carry any responsibility for the conclusions presented herein. We also thank Diane Johnson and Charles Knaack of the WSU Geoanalytical Laboratory, who generated many of the data used in this paper. JMVF research over the years has been supported by Associated Western Universities, Inc., the Department of Energy, and NSF, most recently under EAR-9909700 to J.A.W. The manuscript was improved by the helpful reviews of Mike Dungan, Nancy McMillan and Brad Singer.

REFERENCES

Aldrich, M. J., Jr (1986). Tectonics of the Jemez lineament in the Jemez Mountains and Rio Grande rift. *Journal of Geophysical Research* **91**, 1753–1762.

Aldrich, M. J., Jr & Dethier, D. P. (1990). Stratigraphic and tectonic evolution of the northern Española basin, Rio Grande rift, New Mexico. *Geological Society of America Bulletin* **102**, 1695–1705.

Allègre, C., Michard, A. & Allègre, F. (1986). Europe and trace element geochemistry of Colorado Plateau volcanics. *Geochimica et Cosmochimica Acta* **50**, 2735–2750.

Bailey, R. A., Smith, R. L. & Ross, C. S. (1969). Stratigraphic nomenclature of volcanic rocks in the Jemez Mountains, New Mexico. *US Geological Survey Bulletin* **1274-P**, 1–19.

Baldridge, W. S. (1979). Petrology and petrogenesis of Plio-Pleistocene basaltic rocks from the central Rio Grande rift, New Mexico, and their relation to rift structure. In Riecker, R. E., ed. *Rio Grande Rift: Tectonics and Magmatism*. Washington, DC: American Geophysical Union, pp. 323–353.

Baldridge, W. S. (2004). Pliocene–Quaternary volcanism in New Mexico and a model for genesis of magmas in continental extension. In: Mack, G. H. & Giles, K. A., eds. *The Geology of New Mexico: a Geologic History*. New Mexico Geological Society Special Publication **11**, 313–330.

Baldridge, W. S., Damon, P. E., Shafiqullah, M. & Bridwell, R. J. (1980). Evolution of the central Rio Grande rift, New Mexico: new potassium–argon ages. *Earth and Planetary Science Letters* **51**, 309–321.

Baldridge, W. S., Olsen, K. H. & Callender, J. F. (1984). Rio Grande rift: problems and perspectives. In Baldridge, W. S., Dickerson, P. W., Riecker, R. E. & Zidek, J., eds. *Rio Grande Rift: Northern New Mexico*. New Mexico Geological Society 35th Field Conference Guidebook, pp. 1–12.

Bohrson, W. A. & Spera, F. J. (2001). Energy-constrained open-system magmatic processes II: application of energy-constrained assimilation–fractional crystallization (EC-AFC) model to magmatic systems. *Journal of Petrology* **42**, 1019–1041.

Brookins, D. G. & Laughlin, A. W. (1984). Rb–Sr geochronological investigation of Precambrian samples from deep geothermal drill holes, Lemon Hill, New Mexico. *Journal of Volcanology and Geothermal Research* **15**, 43–59.

Clarkson, G. & Reiter, M. (1984). Analysis of terrestrial heat-flow profiles across the Rio Grande rift and southern Rocky Mountains in northern New Mexico. In Baldridge, W. S., Dickerson, P. W., Riecker, R. E. & Zidek, J., eds. *Rio Grande Rift: Northern New Mexico*. New Mexico Geological Society 35th Field Conference Guidebook, pp. 39–44.

Class, C. & Goldstein, S. L. (1997). Plume–lithosphere interactions in the ocean basins: constraints from the source mineralogy. *Earth and Planetary Science Letters* **150**, 245–260.

Class, C., Goldstein, S. L., Altherr, R. & Bachèlery, P. (1998). The process of plume–lithosphere interactions in the ocean basins—the case of Grande Comore. *Journal of Petrology* **39**, 881–903.

Class, C., Goldstein, S. L. & Shirey, S. B. (1998). Plume–lithosphere interactions in the ocean basins: new constraints from Os isotopes in Grande Canarie lavas. *EOS Transactions, American Geophysical Union* **79/45**, 949.

Class, C., Goldstein, S. L. & Shirey, S. B. (1999). Plume–lithosphere interactions in the ocean basins: new constraints from Os isotopes in Grande Canarie lavas. *EOS Transactions, American Geophysical Union* **80/46**, 1193.

Dalpé, C. & Baker, D. R. (2000). Experimental investigation of large-ion lithophile elements, high field strength element- and rare-earth element-partitioning between calcic amphibole and basaltic melt: the effects of pressure and oxygen fugacity. *Contributions to Mineralogy and Petrology* **140**, 233–250.

Davidson, J. P., Hughes-Saar, N. D. & Wilson, M. (1993). The geochemistry of the igneous rock suite of St. Martin, Northern Lesser Antilles. *Journal of Petrology* **34**, 839–866.

DePaolo, D. J. (1981). Trace element and isotopic effects of combined wallrock assimilation and fractional crystallization. *Earth and Planetary Science Letters* **144**, 153–168.

Dethier, D. P. (1997). Geology of White Rock quadrangle, Los Alamos and Santa Fe Counties, New Mexico. *New Mexico Bureau of Mines and Mineral Resources, Geologic Map* **73**, scale 1:24 000.

Dethier, D. P., Abrich, M. J., Jr & Shafiqullah, M. (1986). New K–Ar ages for Miocene volcanic rocks from the northeastern Jemez Mountains and Española Basin, New Mexico. *Geologic Map* **47**, 12–14.

Daeckel, K., Yuan, H. & Zuck, R. (2001). Early structural Proterozoic lithosphere of the Rocky Mountain region. *GSA Today* **11/12**, 4–9.

Dunbar, N. W. & Hervig, R. L. (1992). Volatile and trace element composition of melt inclusions from the Lower Bandelier Tuff: implications for magma chamber processes and eruptive style. *Journal of Geophysical Research* **97**, 15151–15170.

Dunker, K. E., Wolff, J. A., Harmon, R. S., Leat, P. T., Dickin, A. P. & Thompson, R. N. (1983). Discrete mantle and crustal components in lavas of the NW Cerros del Rio volcanic field, Rio Grande rift, New Mexico. *Contributions to Mineralogy and Petrology* **108**, 331–345.

Dungan, M. A., Lindstrom, M. M., McMillan, N. J., Moorbath, S., Hoefs, J. & Huskes, E. (1986). Open system magmatic evolution of the Taos Plateau volcanic field, northern New Mexico. I. The petrology and geochemistry of the Servilleta Basalt. *Journal of Geophysical Research* **91**, 5999–6028.

Dungan, M. A., Thompson, R. A., Stormer, J. S. & O'Neill, J. M. (1989). Excursion 18B: Rio Grande rift volcanism, northeastern Jemez zone, New Mexico. *New Mexico Bureau of Mines and Mineral Resources, Memoir* **46**, 455–486.

Eichelberger, J. C. & Koch, F. G. (1979). Lithic fragments in the Bandelier Tuff, Jemez Mountains, New Mexico. *Journal of Volcanology and Geothermal Research* **5**, 117–134.

Ellison, R., Wolff, J. A. & Gardner, J. N. (1996). Outline of the petrology and geochemistry of the Keres Group lavas and tuffs. In: Goff, F., Kues, B. S., Rogers, M. A., McLaughlin, L. D. & Gardner, J. N. (eds), *The Jemez Mountains Region. New Mexico Geological Society, 47th Field Conference Guidebook*, pp. 237–242.

Gardner, J. N. (1985). Tectonic and petrologic evolution of the Keres Group: implications for the development of the Jemez volcanic field, New Mexico. Ph.D. dissertation, University of California, 294 pp.

Gardner, J. N., Goff, F., Garcia, S. & Hagan, R. C. (1986). Stratigraphic relations and lithologic variations in the Jemez volcanic field, New Mexico. *Journal of Geophysical Research* **91**, 1763–1778.

Ghiorso, M. S. & Sack, R. O. (1995). Chemical mass transfer in magmatic processes. IV. A revised and internally consistent thermodynamic model for the interpolation and extrapolation of liquid–solid equilibria in magmatic systems at elevated temperatures and pressures. *Contributions to Mineralogy and Petrology* **119**, 197–212.

Gibson, S. A., Thompson, R. N., Leat, P. T., Morrison, M. A., Hendry, G. L., Dickin, A. P. & Mitchell, J. G. (1993). Ultrapotassic magmas along the flanks of the Oligo-Miocene Rio Grande rift, USA: monitors of the zone of lithospheric mantle extension and thinning beneath a continental rift. *Journal of Petrology* **34**, 187–228.

Goff, F., Gardner, J. N., Baldridge, W. S., Hulen, J. B., Nielson, D. L., Vigil, D., Heiken, G., Dungan, M. A. & Broxton, D. (1989). Excursion 17B: volcanic and hydrothermal evolution of Valles caldera and Jemez volcanic field. *New Mexico Bureau of Mines and Mineral Resources, Memoir* **46**, 381–444.

Goff, F., Gardner, J. N. & Valentine, G. (1990). Geology of St. Peter's Dome area, Jemez Mountains, New Mexico. *New Mexico Bureau of Mines and Mineral Resources, Geologic Map* **69**, scale 1:24 000.

Hallett, R. B. & Kyle, P. R. (1993). XRF and INAA determinations of major and trace elements in Geological Survey of Japan igneous and sedimentary rock standards. *Geostandards Newsletter* **17**, 127–143.

Hart, S. R. (1984). A large-scale isotope anomaly in the southern hemisphere mantle. *Nature* **309**, 753–757.

Hart, S. R. & Dunn, T. (1993). Experimental cpx/melt partitioning of 24 trace elements. *Contributions to Mineralogy and Petrology* **113**, 1–8.

Hauri, E. H. (1996). Major-element variability in the Hawaiian mantle plume. *Nature* **382**, 415–419.

Hauri, E. H., Wagner, T. P. & Grove, T. L. (1994). Experimental and natural partitioning of Th, U, Pb and other trace elements between garnet, clinopyroxene and basaltic melts. *Chemical Geology* **117**, 149–166.

Hildreth, W. E. (1981). Gradients in silicic magma chambers: implications for lithospheric magmatism. *Journal of Geophysical Research* **86**, 10153–10192.

Hirschmann, M. M. & Stolper, E. M. (1996). A possible role for garnet pyroxenite in the origin of the "garnet signature" in MORB. *Contributions to Mineralogy and Petrology* **124**, 185–208.

Hofmann, A. W., Jochum, K. P., Seufert, M. & White, W. M. (1986). Nb and Pb in oceanic basalts: new constraints on mantle evolution. *Earth and Planetary Science Letters* **79**, 33–45.

Hulen, J. B. & Gardner, J. N. (1989). Field geologic log for Continental Scientific Drilling Program Corehole VC-2B, Valles caldera, New Mexico. *US Department of Energy, Open File Report* **DOE/ER/13196-4 ESL-89025-TR**, 92 pp.

Irvin, G. A. & Obradovich, J. D. (1994). $^{40}Ar/^{39}Ar$ age constraints for the Jaramillo normal subchron and the Matuyama–Brunhes geomagnetic boundary. *Journal of Geophysical Research* **99**, 2943–2944.

Johnson, C. M. & Beard, B. L. (1993). Evidence from hafnium isotopes for ancient suboceanic mantle beneath the Rio Grande rift. *Nature* **362**, 441–444.

Johnson, D. M., Hooper, P. R. & Conrey, R. M. (1999). XRF analysis of rocks and minerals for major and trace elements on a single low dilution Li-tetraborate fused bead. *Advances in X-ray Analysis* **41**, 843–867.

Johnson, K. T. H. (1994). Experimental clinopyroxene and garnet melt partitioning of REE and other trace elements at high pressures: petrogenetic implications. *Mineralogical Magazine* **58A**, 453–455.

Kerkhoven, K. E., *et al.*, CD-ROM Working Group (2002). Structure and evolution of the lithosphere beneath the Rocky Mountains: initial results from the CD-ROM experiment. *GSA Today* **12/3**, 4–10.

Kinard, L., Carnahan, S. & Hooper, P. R. (1994). Trace element analysis of rocks and minerals by ICP-MS. *Open File Report, Department of Geology, Washington State University.*

Lassiter, J. C., Hauri, E. H., Reiners, P. W. & Garcia, M. O. (2000). Generation of Hawaiian post-erosional lavas by melting of a mixed

lherzolite/pyroxenite source. *Earth and Planetary Science Letters* **178**, 269–284.

LeTourneau, L., Hersig, R. L. & Hollocher, J. R. (1996). Trace-element partitioning between amphibole, phlogopite, and basaltic melt. *Earth and Planetary Science Letters* **135**, 13–30.

Loughlin, A. W., Eddy, A. C., Laney, R. & Mersh, M. J. (1993). Geology of the Trujillo Hill, New Mexico, hot dry rock site. *Journal of Volcanology and Geothermal Research* **15**, 21–41.

Lum, P. L., Thompson, R. N., Morrison, M. A., Hendry, G. L. & Dickin, A. P. (1989). Compositionally diverse Miocene–Recent rift-related magmatism in northwest Colorado, partial melting, and mixing of mafic magmas from three different asthenospheric and lithospheric mantle sources. *Journal of Petrology, Special Lithosphere Issue*, 551–577.

Lum, P. L., Thompson, R. N., Dickin, A. P., Morrison, M. A. & Hendry, G. L. (1989). Quaternary volcanism in NW Colorado: implications for the roles of asthenosphere and lithosphere in the genesis of continental basalts. *Journal of Volcanology and Geothermal Research* **37**, 299–310.

Lum, P. L., Thompson, R. N., Morrison, M. A., Hendry, G. L. & Dickin, A. P. (1990). Geochemistry of mafic lavas in the early Rio Grande rift, Yampa Mountain, Colorado, USA. *Chemical Geology* **81**, 23–43.

Manley, K. (1962). Geologic map of the Cañones quadrangle. *US Geological Survey, Miscellaneous Field Studies, Map* **MF-1440**, scale 1:24 000.

McDonough, W. F. & Sun, S.-s. (1995). The composition of the Earth. *Chemical Geology* **120**, 223–253.

McMillan, N. J. (1991). Temporal and spatial magmatic evolution of the Rio Grande rift. In: Mack, G. (ed.), *Las Cruces Country II, New Mexico Geological Society, 42th Field Conference Guidebook*, pp. 107–116.

McMillan, N. J. & Dungan, M. A. (1988). Open system magmatic evolution of the Late Pliocene volcanic field, northern New Mexico: 3. Petrology and geochemistry of andesite and dacite. *Journal of Petrology* **29**, 527–557.

McMillan, N. J., Dickin, A. P. & Haag, D. (2000). Evolution of magma source regions in the Rio Grande rift, southern New Mexico. *Geological Society of America Bulletin* **112**, 1592–1593.

Morgan, P. & Golombek, M. P. (1984). Factors controlling the phases and styles of extension in the northern Rio Grande rift. In: Baldridge, W. S., Dickerson, P. W., Riecker, R. E. & Zaleck, J. (eds), *Rio Grande Rift: Northern New Mexico, New Mexico Geological Society, 35th Field Conference Guidebook*, pp. 13–19.

Morgan, P., Seager, W. R. & Golombek, M. P. (1985). Cenozoic thermal, mechanical and tectonic evolution of the Rio Grande rift. *Journal of Geophysical Research* **91**, 6263–6276.

Nelson, D. L. & Hulen, J. B. (1984). Internal geology and evolution of the Redondo dome, Valles caldera, New Mexico. *Journal of Geophysical Research* **89**, 8693–8711.

Pazzaglia, F. J., Woodward, L. A., Lucas, S. G., Anderson, O. J., Wegmann, K. W. & Lucas, J. W. (1999). Phanerozoic geologic evolution of the Albuquerque area. In: Pazzaglia, F. J. & Lucas, S. G. (eds), *Albuquerque Geology, New Mexico Geological Society, 50th Field Conference Guidebook*, pp. 97–114.

Perry, F. V., Baldridge, W. S. & DePaolo, D. J. (1987). Role of asthenosphere and lithosphere in the genesis of late Cenozoic basaltic rocks from the Rio Grande rift and adjacent regions of the southwestern United States. *Journal of Geophysical Research* **92**, 9193–9213.

Reiners, P. W. & Nelson, B. K. (1998). Temporal-compositional-isotopic trends in rejuvenated-stage magmas of Kauai, Hawaii, and implications for mantle melting processes. *Geochimica et Cosmochimica Acta* **62**, 2347–2368.

Self, S., Goff, F., Gardner, J. N., Wright, J. V. & Kite, W. M. (1986). Explosive rhyolite volcanism in the Jemez Mountains: vent locations, caldera development and relation to regional structure. *Journal of Geophysical Research* **91**, 1779–1798.

Shaw, C. A. & Karlstrom, K. E. (1999). The Yavapai–Mazatzal crustal boundary in the southern Rocky Mountains. *Rocky Mountain Geology* **34**, 37–52.

Sigmarsson, O., Carn, S. & Carracedo, J. C. (1998). Systematics of U-series nuclides in primitive lavas from the 1730–36 eruption on Lanzarote, Canary Islands, and implications for the role of garnet pyroxenites during oceanic basalt formation. *Earth and Planetary Science Letters* **162**, 137–151.

Singer, B. S. & Kudo, A. M. (1986). Assimilation by normal crystallization of Paleozoic Group rocks in the northwestern Jemez Volcanic Field, New Mexico. *Contributions to Mineralogy and Petrology* **94**, 374–386.

Smith, R. L. (1979). Ash-flow magmatism. In: Chapin, C. E. & Elston, W. E. (eds), *Ash-flow Tuffs, Geological Society of America, Special Papers* **180**, 5–28.

Smith, R. L., Bailey, R. A. & Ross, C. S. (1970). Geologic map of the Jemez Mountains, New Mexico. *US Geological Survey, Miscellaneous Geological Investigations, Map* **I-571**, scale 1:250 000.

Spath, A., le Roex, A. P. & Duncan, R. A. (1996). Trace element and Sr–Nd–Pb–Ar isotope evidence for the origin of the Comoros archipelago, western Indian Ocean: petrogenesis and mantle source characteristics. *Journal of Petrology* **37**, 961–991.

Spath, A., le Roex, A. P. & Opiyo-Akech, N. (2001). Plume–lithosphere interaction and the origin of continental rift-related alkaline volcanism—the Chyulu Hills volcano, southern Kenya. *Journal of Petrology* **42**, 765–787.

Spell, T. L. & Kyle, P. R. (1989). Petrogenesis of Valle Grande Member rhyolites, Valles caldera, New Mexico: implications for evolution of the Jemez Mountains magmatic system. *Journal of Geophysical Research* **94**, 10379–10396.

Spell, T. L., Harrison, T. M. & Wolff, J. A. (1990). $^{40}Ar/^{39}Ar$ dating of the Bandelier Tuff and San Diego Canyon ignimbrites: temporal constraints on magmatic evolution. *Journal of Volcanology and Geothermal Research* **43**, 175–193.

Spell, T. L., Kyle, P. R., Thidwell, M. T. & Campbell, A. R. (1993). Isotopic and geochemical constraints on the origin and evolution of post-collapse rhyolites in the Valles caldera, New Mexico. *Journal of Geophysical Research* **98**, 19723–19739.

Spell, T. L., Kyle, P. R. & Baker, J. (1996). Geochronology and geochemistry of the Cerro Toledo Rhyolite. In: Goff, F., Kues, B. S., Rogers, M. A., McFadden, L. D. & Gardner, J. N. (eds), *The Jemez Mountains Region, New Mexico Geological Society, 47th Field Conference Guidebook*, pp. 263–268.

Spera, F. J. & Bohrson, W. A. (2001). Energy-constrained open-system magmatic processes I: general model and energy-constrained assimilation and fractional crystallization (EC-AFC) formulation. *Journal of Petrology* **42**, 999–1018.

Stimac, J. A. (1996). Hornblende-dacite pumice in the Otowi Member of the Bandelier Tuff: implications for magma chamber and eruptive processes. In: Goff, F., Kues, B. S., Rogers, M. A., McFadden, L. D. & Gardner, J. N. (eds), *The Jemez Mountains Region, New Mexico Geological Society, 47th Field Conference Guidebook*, pp. 269–274.

Stix, J. & Gorton, M. P. (1991). Replenishment and crystallisation in epicontinental silicic magma chambers: evidence from the Bandelier magmatic system. *Journal of Volcanology and Geothermal Research* **55**, 201–215.

Stix, J., Goff, F., Gorton, M. P., Heiken, G. & Garcia, S. R. (1988). Restoration of compositional zonation in the Bandelier silicic magma

chamber between two caldera-forming eruptions: geochronology and origin of the Cerro Toledo Rhyolite, Jemez Mountains, New Mexico. *Journal of Geophysical Research* **93**, 6129–6147.

Sun, S.-s., 1980. Lead isotopic study of young volcanic rocks from mid-ocean ridges, ocean islands and island arcs. *Philosophical Transactions of the Royal Society of London* **297**, 409–445.

Sun, S.-s. & McDonough, W. F., 1989. Chemical and isotopic systematics of oceanic basalts: implications for mantle composition and processes. In: Saunders, A. D. & Norry, M. J., eds. *Magmatism in the Ocean Basins. Geological Society, London, Special Publication* **42**, 313–345.

Taylor, H. P., Jr., 1968. The effects of assimilation of country rocks by magmas on $^{18}O/^{16}O$ and $^{87}Sr/^{86}Sr$ systematics in igneous rocks. *Earth and Planetary Science Letters* **47**, 243–254.

Thompson, R. N., Morrison, M. A., Hendry, G. L. & Parry, S. J., 1984. An assessment of the relative roles of crust and mantle in magma genesis: an elemental approach. *Philosophical Transactions of the Royal Society of London, Series A* **310**, 549–590.

Turbeville, B. N., Waresback, D. B. & Self, S., 1989. Lava-dome growth and explosive volcanism in the Jemez Mountains, New Mexico: evidence from the Plio-Pleistocene Paja alluvial fan. *Journal of Volcanology and Geothermal Research* **36**, 267–291.

Weaver, B. L., 1991. The origin of ocean island basalt end-member compositions: trace element and isotope constraints. *Earth and Planetary Science Letters* **104**, 381–397.

Wolfe-Gabriel, G., Laughlin, A. W., Dobner, D. P. & Heizler, M., 1990. Temporal and geochemical trends of lavas in White Rock Canyon and the Pajarito Plateau, Jemez volcanic field, New Mexico, USA. In: Goff, F., Kues, B. S., Rogers, M. A., McFadden, L. D. & Gardner, J. N., eds. *The Jemez Mountains Region. New Mexico Geological Society, 41st Field Conference Guidebook*, pp. 251–261.

Wolfe-Gabriel, G., Warren, R. G., Gob, C., Goff, F., Broxton, D., Vaniman, D., Peters, L. & Naranjo, A., 2001. Periodicity and distribution of volcanism in the Pajarito Plateau, Rio Grande rift north-central New Mexico. *US Geological Survey Open-File Report* **03-369**, 7.

Wolff, J. A. & Gardner, J. N., 1995. Is the Valles caldera entering a new cycle of activity? *Geology* **23**, 411–414.

Wolff, J. A. & Ramos, F. C., 2003. Pb isotope variations among Bandelier Tuff feldspars: no evidence for a long-lived silicic magma chamber. *Geology* **31**, 549–550.

Wolff, J. A., Ramos, F. C. & Davidson, J. P., 1999. Sr isotope disequilibrium during differentiation of the Bandelier Tuff: constraints on the crystallization of a large rhyolitic magma chamber. *Geology* **27**, 495–498.

Wolff, J. A., Heiken, G. E. & Ellison, R., 2000. Hybrid origin of Rio Grande rift basaltes. *Geology* **28**, 203–206.

Wolff, J. A., Balsley, S. D. & Gregory, R. T., 2002. Oxygen isotope disequilibrium between quartz and sanidine from the Bandelier Tuff, New Mexico, consistent with a short residence time of phenocrysts in rhyolitic magma. *Journal of Volcanology and Geothermal Research* **116**, 119–135.